Helsinki University of Technology Radio Laboratory Publications
Teknillisen korkeakoulun Radiolaboratorion julkaisuja
Espoo, March 2005 REPORT S 267

STUDIES ON MICROWAVE ANTENNAS: PASSIVE INTERMODULATION DISTORTION IN ANTENNA STRUCTURES AND DESIGN OF MICROSTRIP ANTENNA ELEMENTS

Sami Hienonen

Dissertation for the degree of Doctor of Science in Technology to be presented with due permission for public examination and debate in Auditorium S4 at Helsinki University of Technology (Espoo, Finland) on the 18th of March 2005 at 12 o'clock noon.

Helsinki University of Technology
Department of Electrical and Communications Engineering
Radio Laboratory

Teknillinen korkeakoulu
Sähkö- ja tietoliikennetekniikan osasto
Radiolaboratorio

Distribution:

Helsinki University of Technology

Radio Laboratory

P.O.Box 3000

FI-02015 TKK

Tel. +358-9-451 2252

Fax. +358-9-451 2152

ISBN 951-22-7484-1 (print)
ISBN 951-22-7485-X (pdf)

ISSN 1456-3835

Otamedia Oy

Espoo 2005

Preface

The work for this thesis has been done at the Radio Laboratory of Helsinki University of Technology during 1997–2004. The work has been financed by Academy of Finland, National Technology Agency of Finland (TEKES), Nokia Networks and Filtronic LK. My postgraduate studies have also been supported financially by Jenny and Antti Wihuri Foundation, Nokia Foundation, Foundation for Technology and Emil Aaltonen Foundation. I highly appreciate their support.

I am grateful to my supervisor Professor Antti Räisänen for the guidance and support. Professor Pertti Vainikainen and Docent Arto Lehto have given valuable advices and ideas during the work. I would also like to thank Mr. Viatcheslav Golikov for the collaboration and many fruitful discussions. I acknowledge the pre-examiners Dr. Jussi Rahola and Mr. Adrian Rawlins for their many useful comments and suggestions.

I wish to thank my colleagues in the Radio Laboratory for the pleasant and cooperative working environment. Dr. Juha Mallat deserves special thanks for his inexhaustible source of humour and for the encouragement. I would also like to thank the laboratory technicians Eino Kahra and Lauri Laakso for helping to construct numerous prototypes.

Finally, I want to thank my wife Heini and our children Elli-Maija, Helka and Martta for their support and encouragement. Especially, they evidenced an enormous amount of patience and understanding during the last month of writing the thesis manuscript, which happened to coincide with the UEFA European Championship football tournament.

Espoo, January 12, 2005

Sami Hienonen

Abstract

Passive intermodulation (PIM) measurements of antennas and the design of dual-polarised microstrip antenna elements are investigated in this thesis. The emphasis is on the development of a passive intermodulation source localisation method and on the studies of the PIM source behaviour under various impedance loading conditions.

Passive intermodulation distortion can be harmful in wireless communication systems where the difference between the transmitted and the received power is large such as in GSM base stations. One of the most critical components is the antenna. As the antennas become more complex, the risk of getting excessive PIM distortion increases. Therefore, the antenna designer needs to have knowledge about the PIM phenomenon and proper tools to investigate various antenna structure configurations.

The concept of PIM near-field measurement is introduced and the implementation of the equipment for the GSM 900 frequency band is presented. The performance of the scanner is analysed and demonstrated with measurements. The scanner is capable of locating PIM sources in antennas and other open structures down to -110 dBm when the transmitted power is 43 dBm. The limiting factors of the scanner sensitivity are considered and several sensitivity measurements are performed. An analysis of the impedance loading effects on PIM measurements is carried out. The conducted measurements support the theory that the loading impedance effects can be several decibels, when the source or load return loss is less than 20 dB, which is the case with many filters and antennas used in base stations.

Dual-polarised antenna elements are needed in various array antenna applications. Two compact antenna element designs with moderate bandwidth and dual polarisation are introduced in the 12 GHz frequency band. The elements use a dual-resonant structure in order to achieve an impedance bandwidth of 16 % ($L_{\mathrm{retn}} > 10$ dB). The arrangement of the antenna feeds results in an isolation of 35 dB between the ports.

Contents

List of Publications

[P1] S. Hienonen, V. Golikov, P. Vainikainen, and A. V. Räisänen, "Near-field scanner for the detection of passive intermodulation sources in base station antennas," *IEEE Transactions on Electromagnetic Compatibility*, vol. 46, no. 4, Nov. 2004, pp. 661–667.

[P2] S. Hienonen, P. Vainikainen, and A. V. Räisänen, "Sensitivity measurements of a passive intermodulation near-field scanner," *IEEE Antennas and Propagation Magazine*, vol. 45, no. 4, Aug. 2003, pp. 124–129. Based on the paper in *Proceedings of the 24th Annual Meeting & Symposium of the Antenna Measurement Techniques Association (AMTA 2002)* (Ref. [80]).

[P3] S. Hienonen and A. V. Räisänen, "Effect of the load impedance on passive intermodulation measurements," *Electronics Letters*, vol. 40, no. 4, Feb. 2004, pp. 245–247.

[P4] S. Hienonen and A. V. Räisänen, "Passive intermodulation near-field measurements on microstrip lines," *Proceedings of the 34th European Microwave Conference EuMC 2004*, Amsterdam, Oct 12–14, 2004, pp. 1041–1044.

[P5] S. Hienonen, A. Lehto, and A. V. Räisänen, "Simple broadband dual-polarized aperture-coupled microstrip antenna," in *Proceedings of the IEEE Antennas and Propagation Society International Symposium 1999*, vol. 2, Orlando, FL, July 11–16, 1999, pp. 1228–1231.

[P6] S. Hienonen, A. Lehto, and A. V. Räisänen, "Compact wide-band dual-polarized microstrip antenna," *Microwave and Optical Technology Letters*, vol. 28, no. 6, Mar. 2001, pp. 396–398.

The publications have been mainly written and the theoretical and experimental work has been mainly conducted by the author. In paper [P1], Viatcheslav Golikov has contributed as a team member in the development of the passive intermodulation scanner. He has also conducted some preliminary measurements. Pertti Vainikainen, Arto Lehto and Antti Räisänen have been the supervisors of the papers.

Symbols

a	real coefficient, a-spot radius
A_{a}	apparent contact area
A_{b}	load bearing area
A_{c}	conducting area
B	bandwidth
f	frequency
$\mathcal{F}$	Fourier transform
i, I	current
i, k, K	non-negative integer
k_{B}	bandwidth enlargement factor
l	distance
L_{retn}	return loss
m	integer
M	non-negative integer
N, q	non-negative integer
P	power
Q	quality factor
r	real number
R_{c}	constriction resistance
S	real number, ≥ 1
t	time
T	temperature
v	voltage
V	amplitude
x	transmitted signal
Z	impedance
α	temperature coefficient of resistivity
β	phase constant (imaginary part of the propagation constant)
Γ	reflection coefficient
ε_{r}	relative permittivity
θ	phase
λ	wavelength, thermal conductivity
ρ	resistivity

Abbreviations

ant	antenna
AUT	antenna under test
BJT	bipolar junction transistor
cal	calibration signal
dc	direct current
DUT	device under test
FET	field effect transistor
GSM	Global system for mobile communications
GSM 900	GSM for 900 MHz frequency band
IM	intermodulation
MEMS	micro-electromechanical system
PA	power amplifier
PIM	passive intermodulation
PTFE	polytetrafluoroethylene
RF	radio frequency
Rx	receive
SAR	synthetic aperture radar
SEM	scanning electron microscope
Tx	transmit
VNA	vector network analyser
YIG	yttrium iron garnet

1 Introduction

Passive intermodulation (PIM) measurements of antennas and the design of dual-polarised microstrip antenna elements are investigated in this thesis. However, the emphasis is on the development of passive intermodulation measurements at the frequency range of 900 MHz.

1.1 Background

During the last years the number of communication systems and users has increased considerably. Therefore, these systems are designed to use the scarce radio frequency spectrum as efficiently as possible. When multiple closely spaced frequency channels are used for both transmission and reception in a single radio site, the risk of getting interference within or between the systems increases.

Passive intermodulation (PIM) distortion is a phenomenon that may degrade the performance of a multichannel wireless communication system where the difference between the transmitted and the received power is large. Passive intermodulation occurs in passive devices and components that are normally considered to be linear such as cables, connectors and antennas. However, when subject to high enough power, these devices generate intermodulation signals with a level of typically from -180 to -120 dBc. A sketch of a GSM (Global System for Mobile Communications) base station transceiver with two transmitting signals is shown in Fig. 1. Any nonlinear part in the antenna path will generate intermodulation signals that may appear as interference in the receiver.

The work has been motivated by the general tendency to lower the manufacturing costs of antennas by automating the production line and by using inexpensive materials and processes while the base station antennas become more complex. In the same base station antenna package, there can be antennas for three different frequency bands with two polarisations and each antenna consists typically of several antenna elements. In addition, the antennas might be able to perform mechanical or electrical beam tilting. The complexity of the antennas increases the possibility in getting excessive passive intermodulation distortion as the number of metal-to-metal contacts and transmitting signals increase. In a recent study, a number of commercial antennas were found to have a wide spread in their PIM characteristics, which suggests that careless design will result in an unacceptable passive intermodulation distortion level, see Fig. 2 [1].

It has been known for almost seven decades, that metal-to-metal contacts are typical sources of passive intermodulation distortion [2]. The performance can be improved, for example, by using silver plating on the contact surfaces or by using soldered junctions, but sometimes it might be favourable to use mechanical contacts without plating. Therefore, the antenna designer needs to have knowledge about the PIM phenomenon and proper tools to investigate various antenna structure configurations.

The other subject of the thesis is the design of compact dual-polarised microstrip antenna elements for phased array antenna applications with two polarisations. The potential applications include satellite television reception, base station antennas and synthetic aperture radar (SAR) instruments. In these applications, the antenna elements typically have a moderate bandwidth (10–20%) and the copolar radiation pattern should confine to specific limits, antenna return loss should be in the range from 10 to 20 dB and cross-polarisation level from 20 to 25 dB, which are not trivial specifications to fulfil over the whole bandwidth. Furthermore, there will be little

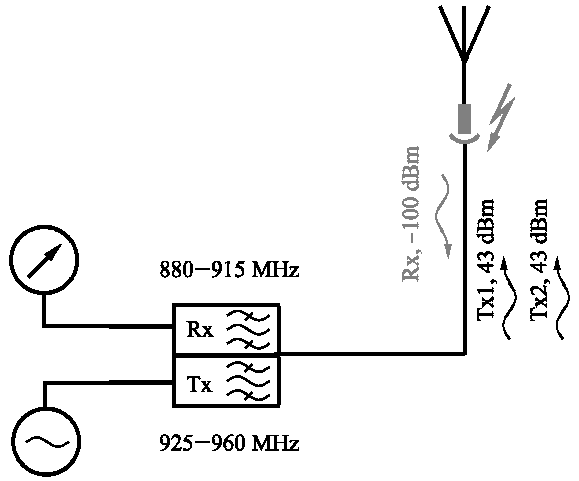

Figure 1. Passive intermodulation source in the antenna path of a GSM base station.

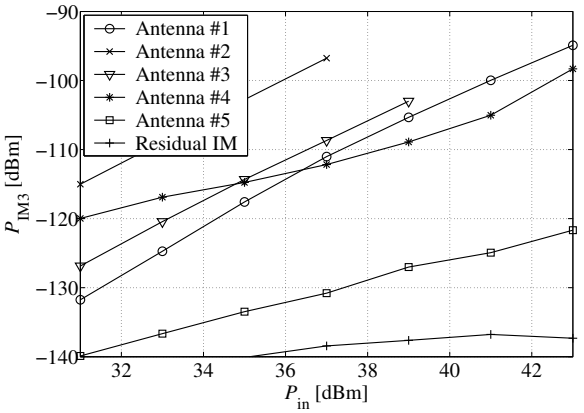

Figure 2. Measured PIM levels of various base station antennas. [1]

space for feed, bias and control networks in a phased-array antenna, which has to be taken into account in the antenna element design.

1.2 Objectives of the work

The main goal of this thesis is to provide new ideas and tools for antenna design with regard to the passive intermodulation phenomenon. Attention is paid to the PIM source localisation and to the behaviour of PIM sources under various impedance loading conditions. The thesis considers GSM base station antennas in the frequency range of 900 MHz (GSM 900), but the principles can be applied to other systems and frequency bands, too. In this thesis, special attention has been paid to microstrip techniques, because they can be utilised both in the implementation of the feeding network as well as in the antenna elements themselves. The dielectric is typically air in outdoor applications whereas microwave substrates can be used in indoor antennas.

The specific application of the microstrip antenna design is the satellite television reception at the frequency band of 10.70–12.75 GHz. The return loss of the antenna element was specified to be better than 10 dB and the cross-polarisation level better than -20 dB. Special attention has been payed to the compactness of the antenna elements so that there will be enough space for the feeding networks.

1.3 Contents of the thesis

The thesis consists of six publications [P1]–[P6] and a summary. The use and applicability of the near-field scanner for the detection of passive intermodulation sources is studied in papers [P1] and [P2]. The effect of the PIM source circuit model on measurements is studied in [P3] and [P4]. Paper [P4] contains also further examples of PIM scanner measurements. Papers [P5] and [P6] contain the description of two different microstrip antenna designs.

The summary part is organised as follows: The problems of passive intermodulation distortion in communication systems are briefly described and some basic theory on the generation of intermodulation products is given in Chapter 2. Chapter 3 contains a literature review about

the physical mechanisms behind the PIM distortion emphasising the time dependency of a PIM signal. General guidelines for designing low-PIM devices are given in Chapter 4. In Chapter 5, the PIM sources are considered as circuit elements whose behaviour under different impedance loadings is studied. PIM source localisation methods are presented and the PIM near-field scanner, the main contribution of the thesis, is introduced in Chapter 6. Considerations on broadband dual-polarised antenna elements are presented in Chapter 7. Finally, the summaries of the publications [P1]–[P6] are given in Chapter 8 and the conclusions in Chapter 9.

2 Passive intermodulation distortion in communication systems

The passive intermodulation distortion has been found problematic in naval, spaceborne, and land mobile communication, as well as in broadcasting systems [3, 4]. The common factors of these systems are that high power signals at many frequencies are used simultaneously and the antennas are compactly packed in an antenna tower or in a satellite. The origin of PIM distortion is typically either a nonlinear metal-to-metal junction or nonlinear material subject to high electric or magnetic field density. These sources of PIM might locate within the antenna paths or in the nearby objects that re-radiate the PIM signals to their surroundings. The interfered receiver can be in-system or belong to another system as shown in Fig. 3. In satellite communications, the critical components are typically reflector surfaces, feed antennas, multiplexers, filters, waveguide flanges, and supporting structures.

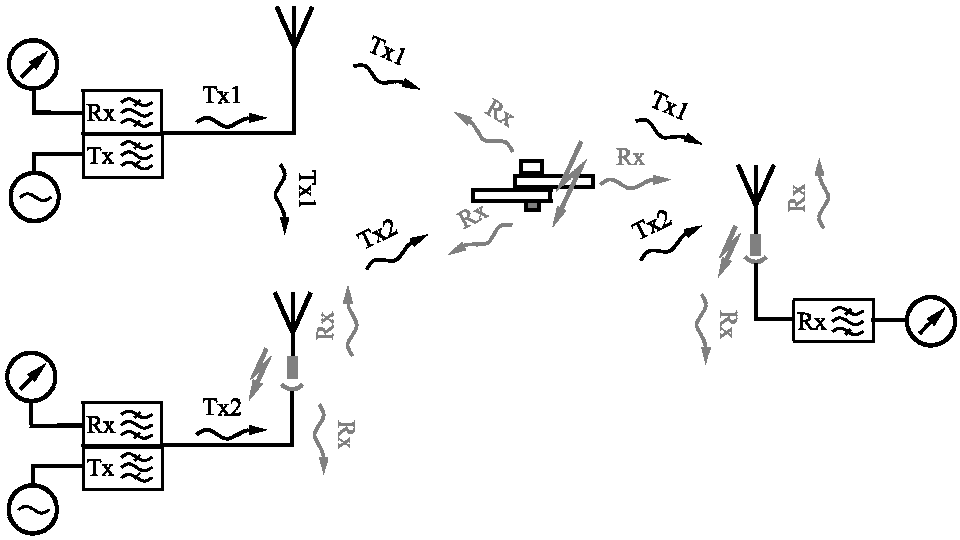

Figure 3. Passive intermodulation generation in multiple systems. Two PIM sources are located in the antenna connectors and one is a loose metal contact in the vicinity of the antennas.

Nowadays communication satellites typically have multiple payloads within a single satellite platform. The large number of possible intermodulation products together with compact antenna mounting structures gives rise to an increased risk of PIM distortion. Therefore, PIM has to be taken into account already in the early system design phase, because at the testing phase the suppression of PIM signals might be too expensive or not possible [5–7]. The satellite system must be tested as an entity, so that large PIM measurement facilities must be used.

2.1 Generation of intermodulation products

Although the Taylor polynomial model is not generally valid for passive intermodulation sources, the generation of intermodulation signals can be understood by applying a multitone stimulus to a nonlinear device that obeys the Taylor polynomial model [8]. The dependency of a current i on the voltage v_s in a memoryless, well-behaving nonlinearity can be approximated with a

Taylor polynomial of degree K:

$$i(v_s) = \sum_{k=0}^{K} a_k v_s^k, \quad a_k = \frac{i^{(k)}(0)}{k!}, \tag{2.1}$$

where $i^{(k)}(0)$ denotes the kth derivative of $i(v_s)$ at $v_s = 0$.

It is known that a nonlinear device generates signals also at other frequencies than the stimulus frequencies. The stimulus consists of a sum of M sinusoids with amplitude v_i, phase θ_i and frequency f_i:

$$v_s = \sum_{i=1}^{M} v_i \cos(\omega_i t + \theta_i), \tag{2.2}$$

$$\omega_i = 2\pi f_i. \tag{2.3}$$

When the phases of the stimulus are to be included in the analysis, it is convenient to use the negative frequency and the complex phasor representation in the calculations. Then, the stimulus becomes

$$v_s = \frac{1}{2} \sum_{i=1}^{M} \left(V_i^* e^{-j\omega_i t} + V_i e^{j\omega_i t} \right) \tag{2.4}$$

$$V_i = v_i e^{j\theta_i}, \tag{2.5}$$

where the asterisk denotes complex conjugate. It can be shown by inserting (2.4) into (2.1) that the output frequencies of the nonlinear device are

$$f_o = \sum_{i=1}^{M} m_i f_i \tag{2.6}$$

where m_i's constitute a set of integers that satisfies

$$N = \sum_{i=1}^{M} |m_i|, \tag{2.7}$$

$$N \leq k, \tag{2.8}$$

$$N \text{ and } k \text{ have the same parity.} \tag{2.9}$$

Conventionally, N is called the order of the intermodulation product. This definition is also used in this thesis. The intermodulation product is generated by the nonlinear term with degree k in (2.1). The requirement for the parity of N and k, implies that only odd degree terms can generate odd order intermodulation products.

The output frequency f_o is called an intermodulation frequency, if $f_o \neq nf_i$ ($n = 0, 1, 2, \ldots$). Every set $\{m_i\}$ that satisfies (2.7)– (2.9) corresponds to an intermodulation product, with the exception that the two sets, where $m_i = -m_i$, correspond to the same intermodulation product. For example, the sets $\{m_i\} = \{\pm 2, \mp 1\}$ correspond to the third order intermodulation product at the frequency of $\pm(2f_1 - f_2)$. It should be noted from (2.7)– (2.9) that also the 5th, 7th, ... degree polynomial terms contribute to this third order intermodulation product.

In many cases, the most important intermodulation products are those that fall closest to the

stimulus frequencies. This gives an additional constraint to the set $\{m_i\}$. The in-band intermodulation products are those that satisfy the relation [5]

$$\sum_{i=1}^{M} m_i = 1. \tag{2.10}$$

If a certain frequency band with a lower and upper bounds f_{L} and f_{H} is considered, then also the following constraint must be satisfied

$$f_L \leq \sum_{i=1}^{M} m_i f_i \leq f_H. \tag{2.11}$$

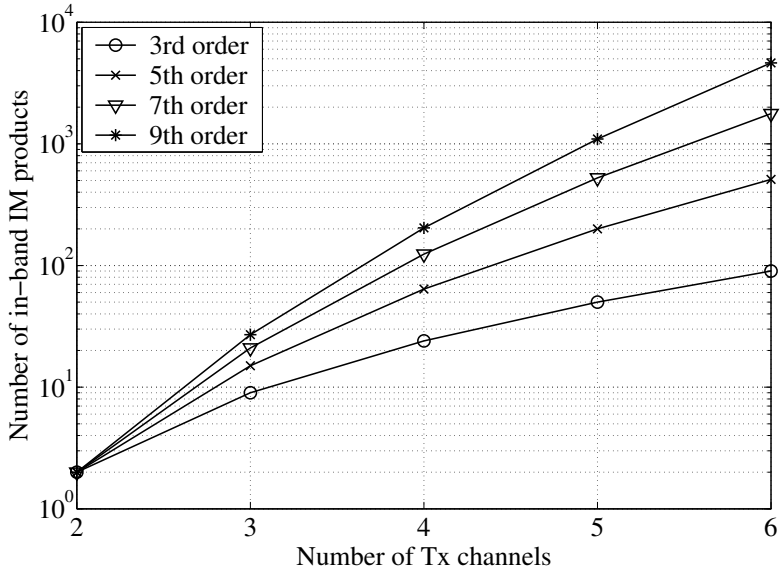

Figure 4. Number of in-band intermodulation products as a function of the channel count.

The number of in-band intermodulation products can be calculated using (2.7)– (2.10). It can be seen from Fig. 4 that the number grows very fast as the channel count and the intermodulation product order are increased. However, depending on the frequencies of the transmitted signals, some different intermodulation products can fall to the same intermodulation frequency.

As an example, let us consider the case with a two-carrier stimulus at the frequencies of f_1 and f_2 ($f_1 < f_2$) and its lower third order in-band intermodulation signal. That is, $M = 2$ and $N = 3$. It is found that only the set $\{m_i\} = \{2, -1\}$ satisfies (2.7)–(2.10) and the requirement for the lower frequency band.

2.1.1 On the order of intermodulation product

An alternative definition for the order of an intermodulation product is sometimes used for the purpose of modelling and analysing intermodulation signals [8, 9]. In this definition, the order of an intermodulation product and the degree of the polynomial term that generates the intermodulation product are equal.

The stimulus in (2.4) can be written as

$$v_s = \frac{1}{2} \sum_{\substack{i=-M \\ i \neq 0}}^{M} V_i e^{j\omega_i t} \tag{2.12}$$

$$V_{-i} = V_i^*, \tag{2.13}$$

$$\omega_{-i} = -\omega_i, \tag{2.14}$$

Then, the output frequencies are

$$f_o = \sum_{\substack{i=-M \\ i \neq 0}}^{M} m_i' f_i, \tag{2.15}$$

where m_i's constitute a set of non-negative integers.

The alternative definition for the order of an intermodulation product is

$$N' = \sum_{\substack{i=-M \\ i \neq 0}}^{M} m_i', \tag{2.16}$$

where the relation between the sets $\{m_i\}$ and $\{m_i'\}$ is

$$m_i = -m_{-i}' + m_i', \quad i > 0. \tag{2.17}$$

Thus, the intermodulation product using the definition in the preceding section splits now into several products. For example, the set $\{m_i'\} = \{1,0,2,0\}$ corresponds to the set $\{m_i\} = \{2, -1\}$, when the polynomial degree is $k = 3$. Here, $N' = N = 3$. However, when $k = 5$, there are two sets $\{m_i'\} = \{2,0,2,1\}$ and $\{m_i'\} = \{1,1,3,0\}$ that satisfy (2.17). Now, $N' = 5$.

The sets $\{m_i'\}$ are used in the following section when calculating the amplitude of an intermodulation product.

As stated earlier, when using the definition (2.16), the order of an intermodulation product N' and the polynomial degree k that generated the product are equal:

$$k = N'. \tag{2.18}$$

2.1.2 Amplitude of intermodulation product

The sets $\{m_i'\}$ and the degree k of the polynomial term in (2.1) determine the amplitude of an intermodulation product. This amplitude can be calculated from the multinomial expansion [9]:

$$V_{\mathrm{IM},k} = \frac{a_k\, k!}{2^{k-1}} \sum_{\{m_i'\}} \prod_{\substack{i=-M \\ i \neq 0}}^{M} \frac{V_i^{m_i'}}{m_i'!}. \tag{2.19}$$

As defined in (2.13), complex amplitudes $V_{-i} = V_i^*$ are used in this expression. The sum is carried out over all the sets $\{m_i'\}$ that satisfy (2.6)– (2.9) and (2.17).

Thus, the total amplitude of an Nth order intermodulation product can be calculated by adding (2.19) over $k = N, N+2, N+4, \ldots, K$. For example, with a two-carrier stimulus the amplitude of the lower third order in-band intermodulation signal at the frequency of $2f_1 - f_2$ ($f_1 < f_2$) is

$$\begin{aligned} V_{\mathrm{IM}} = \frac{V_1^2 V_2^*}{64} \big[& 48 a_3 \\ & + 40 a_5 (2|V_1|^2 + 3|V_2|^2) \\ & + 105 a_7 (|V_1|^4 + 4|V_1|^2 |V_2|^2 + 2|V_2|^4) \\ & + 63 a_9 (2|V_1|^6 + 15|V_1|^4 |V_2|^2 + 20|V_1|^2 |V_2|^4 + 5|V_2|^7) \big]. \end{aligned} \tag{2.20}$$

The expression is truncated at $k = 9$.

2.2 Effect of signal bandwidth

Because the communication signals are modulated and thus have a nonzero bandwidth, the intermodulation signals spread in frequency. When two transmitted signals $x_1(t)$ and $x_2(t)$ have an equal bandwidth B, their intermodulation product generated by a kth power nonlinearity will have a bandwidth of kB. The behaviour of the signal spectrum can be demonstrated with the help of the convolution integral because the product of two signals in the time domain corresponds to a convolution integral of the two-sided power density spectrum:

$$\mathcal{F}\{x_1(t)x_2(t)\} = X_1(f) * X_2(f) = \int_{-\infty}^{\infty} X_1(\lambda) X_2(f-\lambda) d\lambda, \tag{2.21}$$

where $\mathcal{F}$ denotes Fourier transform and the uppercase letters indicate Fourier-transformed signals.

If we have two signals at frequencies f_1 and f_2 with a bandwidth B and a constant power density S, then the power density spectrum of an intermodulation product caused by a third power nonlinearity is

$$X_{2f_1-f_2}(f) = \begin{cases} 9a_3^2 S^3/16\,(f+3B/2)^2, & -3B/2 \le f \le -B/2, \\ 9a_3^2 S^3/16\,(3B^2/2 - 2f^2), & -B/2 \le f \le B/2, \\ 9a_3^2 S^3/16\,(f-3B/2)^2, & B/2 \le f \le 3B/2. \end{cases} \tag{2.22}$$

Here, the frequency has been transformed to origin for clarity. Although the spectrum has spreaded, the signal power is still concentrated in the range $-B/2 \le f \le B/2$. The ratio of the power within this range to the total power of the intermodulation signal is $2/3$ or -1.8 dB. Thus, the two-tone test gives slightly pessimistic results compared to the PIM level of a modulated signal PIM.

2.3 Other nonlinear effects in passive devices

Multipactor and corona effects are other nonlinear phenomena that occur in passive devices. They are usually referred as RF (radio frequency) breakdown effects in which electron avalanche takes place, whereas the term passive intermodulation is used for nonlinear effects in contacts and in materials. RF breakdown is strongly dependent on the electric field strength and the gas

pressure and is of concern in space applications under low pressure conditions. However, both the multipaction and the corona effect can be avoided if high enough pressure is established by means of a hermetic sealing of the device.

Multipaction is a resonance phenomenon caused by the avalanche of secondary electrons [10]. It can take place when the mean free path of the electrons is longer than the distance between two metal plates. The electrons accelerated by the electric field release secondary electrons from the other plate, if the energy of the electrons is proper. Then, if the frequency is appropriate, the electric field changes direction and the secondary electrons are accelerated towards the first metal plate releasing more and more electrons. The factors affecting the multipaction are the pressure, frequency, geometry of the device, voltage between the plates, and the surface characteristics of the metal plates. Typical conditions for multipaction to occur are that the gap size is in the millimetre range, the pressure is 10^{-3} mbar or less, the frequency is in the GHz range, and the voltage is one hundred volts or more [11, 12]. The secondary emission and thus multipaction can be affected by applying surface treatment and coating to the metal plates [13].

Corona effect is a local discharge phenomenon that occurs in intermediate pressures, typically between 0.1 and 100 mbar. The corona discharge is caused by electrons that have high enough energy to ionise neutral gas molecules. As an example of the required conditions, corona discharge took place under the pressure from 0.2 to 2.3 mbar and with an RF power of 10 to 20 W at 450 MHz in the tests of an inverted L antenna [14].

3 PIM sources as physical phenomena

The origin of passive intermodulation distortion can be divided into three categories: contact nonlinearities, bulk material nonlinearities, and surface effects. It is known for a long time that metal-to-metal contacts are able to produce extensive PIM distortion [2]. The research on the PIM phenomenon in contacts has mainly been based on the electrical contact theory of dc (direct current) or low-frequency applications [15]. The ferromagnetic materials and ferrites are known to produce PIM distortion due to their nonlinear magnetic behaviour [16, 17]. There has been less research on the surface effects, but for example a rough metal surface has been found to cause detectable PIM distortion [18]. Time variability is characteristic for the PIM distortion generated in contacts, because minor changes in the geometry of the contact may change the PIM level considerably. Nonlinear effects in a bulk material are typically more time-invariant.

There are a number of studies about the generation of PIM distortion in various materials and devices, and also some theoretical models have been proposed. However, currently there does not exist a generally accepted model that could predict the PIM behaviour of a given device. The modelling is difficult, because the microscopic details of a contact at the time of measurement cannot be known exactly. Also, the material purity, imperfections, alloy composition, and surface properties affect the PIM level. In addition, very small nonlinearities can produce observable PIM distortion so that there exists a number of physical processes that can contribute to the experimental results. Many possible physical phenomena behind the PIM distortion found in literature are presented in this chapter. A comprehensive literature survey about the possible physical phenomena behind the PIM distortion can also be found in the report of Foord and Rawlins [19].

3.1 Electrical contacts

Some mostly cited physical phenomena found in electrical contacts are presented in this section. However, it should be noted that the phenomena described in this section depend also on the imperfections in the insulating film and on the metal surfaces. These imperfections give rise also to other possible physical mechanisms that could cause PIM distortion including the non-destructing breakdown through a dielectric film [19].

3.1.1 Mechanical considerations

An electrical contact is a junction between two conductors which is able to carry electric current. Because the conductor surfaces are never flat nor smooth in a microscopic scale, the electrical contact area consists of one or more small areas, spots. The size and number of spots depend not only on the surface geometry but also on the metal hardness and on the force applied to the contact. In fact, an infinitely hard surfaces would touch each other only on three points.

The properties of the contact surfaces have a strong effect on the behaviour of an electrical contact. The surfaces might be plated with an electrically conducting material like silver or gold, or they may be oxidised or contaminated. The contamination can be conducting or insulating and may consist of, for example, hydrocarbons, dust, leftover resin from soldering or particles from the machining of the contact. An electrical contact in a connector is sketched in Fig. 5. The apparent contact area A_a, which is the macroscopic contact area, is typically much larger than the load bearing area A_b, which is the area of the surfaces that is in a mechanical contact. The load

bearing area can be further divided into metallic contact spots, quasi-metallic spots separated by a thin film, and thick film coated areas [15]. The metallic and quasi-metallic spots constitute the conducting area A_c, where the current flow is governed by different physical phenomena. In metallic spots the current depends on the metal conductivity whereas the tunneling effect can dominate the behaviour of the current flow across thin films. The areas of thick film might be insulating, conducting, or they might be subject to an electric breakdown. The conducting area A_c is typically smaller than A_b, but the ratio of A_a, A_b and A_c is difficult to measure for a specific contact.

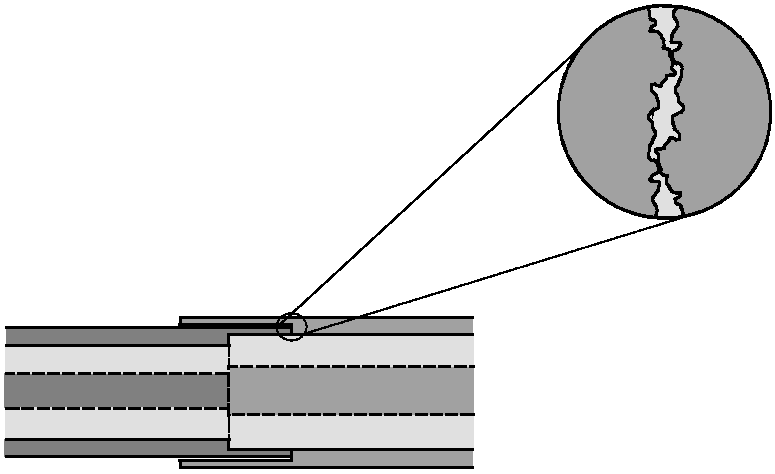

Figure 5. Electrical contact in a connector.

3.1.2 Metallic contacts, a-spots

In general, the conducting area consists of several round or elongated spots. These spots are usually called as a-spots, where the letter a refers to the radius of a circular spot. The size of a-spots can be examined with a scanning electron microscope (SEM). For example, in polished aluminium surfaces with $A_a = 3$ mm^2 the diameter of a-spots varied from 5 μm to 100 μm, although the surfaces had a similar treatment [20, 21]. It was also found that high and unstable contact voltage was associated with the large a-spots.

Because the current has to flow through a narrow spot, there will be additional resistance as compared with the case of an ideal junction. This resistance is called constriction resistance. When two semi-infinite electrodes have a galvanic circular contact with radius a, the constriction resistance at zero frequency is [15]

$$R_c = \frac{\rho_0}{2a}, \tag{3.1}$$

where ρ_0 is the resistivity of the electrodes at a reference temperature of T_0. When there is a film between the contact surfaces, it will cause additional resistance to the contact resistance. There will also be contact capacitance in the junction [22].

It can be seen from (3.1) that for the a-spots in aluminium the constriction resistance is typically on the milliohm order. Skin effect confines the current near surfaces, which is not taken into account in (3.1). As a consequence, the contact resistance increases whereas the constriction resistance may even decrease with increasing frequency [23].

The nonlinearity of the constriction resistance has been given as a possible explanation for PIM distortion in contacts [24]. The nonlinearity is caused by the current that heats the contact, which in turn changes the resistivity. The temperature dependency of resistivity can be approximated with

$$\rho = \rho_0[1 + \alpha(T - T_0)], \tag{3.2}$$

where α is the temperature coefficient of resistivity and T is the temperature.

The current I_c through the a-spot will then be [25]

$$I_c = 4a\sqrt{\frac{\lambda_0}{\rho_0\alpha}}\arctan\left(\frac{V_c}{2}\sqrt{\frac{\alpha}{\rho_0\lambda_0}}\right), \tag{3.3}$$

where V_c is the voltage across the junction and λ_0 is the thermal conductivity of the metal.

Equation (3.3) is valid under steady state conditions when the temperature of the a-spot follows the magnitude of the electric current and the constriction resistance is calculated from (3.1). In order for the intermodulation products to appear, the temperature variation at a rate of the envelope of the transmitted signals must be high enough. This effect could be studied with an electrothermal simulator as has been used to investigate the failure mechanisms of an RF MEMS (micro-electromechanical system) switch [26].

3.1.3 Tunneling effect

The surface of most metals is covered by a thin layer of oxide or other chemical compound. For example, a 10 to 100 Å thick layer of aluminium oxide Al_2O_3 grows spontaneously on a clean aluminium surface. This insulating film causes a potential hill between the metal plates. When the electrons have enough energy to jump over the hill, the phenomenon is called thermionic emission or Schottky effect. If the electrons have lower energy, they tunnel through the potential hill with some probability. The tunneling effect is measurable only for layers that are thinner than 100 Å.

Tunneling effect has been stated many times as a cause of PIM and it has been experimentally investigated in [27–29]. Bond et. al. measured the voltage-current dc curves and the capacitances of several Al–Al_2O_3–Al junctions [29]. As a result they modelled the junction with a linear capacitance and a nonlinear resistance in parallel connected with a linear series resistance. The calculated and measured PIM differed $\pm$15 dB depending on the test sample. It was also found that the dc curves of the junctions changed constantly. The authors explain the discrepancy by a crude approximation of the current density in the square bend where the junction was located. Because of this reasonable agreement of theory and experiments and because the junctions were fabricated under controlled conditions, it is highly probable that the tunneling effect was the reason for the observed PIM levels.

3.1.4 Rusty-bolt phenomenon

When the oxide layer on a metal is porous enough, the oxidisation process does not stop on a specific thickness. Thus, the metal corrodes if the humidity is high enough. Junctions made of iron or steel have been found to produce remarkable PIM distortion in metallic structures in the vicinity of the transmitting antennas [2, 30, 31]. This effect has been called a rusty-bolt effect suggesting that the corroded contacts cause it. A 15 to 30 dB increase in PIM level has been

observed in two independent experiments when steel samples were corroded as compared to clean samples [30, 32]. One experiment was carried out at 5 MHz with $P_{\mathrm{Tx}} = 49$ dBm and the other at 150 MHz with $P_{\mathrm{Tx}} = 47$ dBm. It was suggested that the major phenomenon introducing the non-linearity in corroded junctions would be the semiconducting oxide of the transition metal [32]. However, the experimental results in [33] indicate that the major contributor could be the loose and small-area contacts rather than the corroded junction areas.

3.1.5 Fritting

Fritting is one kind of electric breakdown that typically occurs through 100 Å to 500 Å thick tarnish or contamination films [15]. Fritting can be divided into two categories: A-fritting means a breakdown of the film and results a new a-spot, whereas B-fritting means an enlargement of an existing a-spot. Fritting involves softening or even melting of the contact metal as well as transfer of metal and is therefore an irreversible effect. The mass transport can be caused for example by current induced electromigration or mechanical stress induced metal creep [25, 34]. A-fritting happens typically at contact voltages of few volts and B-fritting may happen in voltages around tens of millivolts [15,25]. Fritting is considered as a dc and low frequency effect and it has been utilised to lower the contact resistance from a MEMS probe to an aluminium pad [35]. One might be tempted to utilise fritting in order to improve the PIM performance of a contact, but the fritting does not necessarily create a stable contact as has been noticed in [21].

3.2 Material nonlinearities

3.2.1 Ferromagnetic materials

Ferromagnetic materials have a large permeability, which saturates under high magnetic fields. The high permeability can be explained by magnetic domains that align parallel when subjected to an external magnetic field [36, 37]. Iron, nickel, cobalt, and some of their alloys, as well as some lanthanide (rare-earth) elements, and certain alloys of magnesium with aluminium and copper are ferromagnetic [38]. The magnetic properties of the material depend on chemical composition, impurities, fabrication, and heat treatment. Permeability of ferromagnetic materials decreases as the frequency increases. Typically the permeabilities of iron and nickel drop to half their normal values in the gigahertz frequency range [37].

Nickel and steel have been found to be significant sources of PIM [16,18,30,39]. In [18], nickel plated centre conductor of a coaxial cable generated a PIM level of -97 dBm at 1.5 GHz with $P_{\mathrm{Tx}} = 44$ dBm. The nonlinearity of nickel at 150 MHz has been analysed in [16]. The authors measured the PIM signal level as a function of the dc magnetic field and contributed the PIM generation to the nonlinear motion of the domain walls. They conclude that the PIM signal level decreases with the domain wall density. In their samples, the PIM level dependency on the input power was quadratic at low dc fields and cubic at high fields. The relative magnetic field orientations of the domains, the dc field, and the RF field as well as the domain structure were found to affect the PIM level.

3.2.2 Ferrimagnetic materials

Ferrimagnetic materials (ferrites) have similar magnetic properties as the ferromagnetic materials, but they are oxides and as such poor conductors. Therefore, they have low losses and retain

their high permeability at microwave frequencies. They are widely used in microwave components like isolators, circulators and phase shifters [40]. Also the YIG (yttrium iron garnet) material used in resonators is a ferrite. The PIM level of a ferrite device is in general higher than that caused by metal contacts, but it has been found that the PIM distortion level can be optimised [17, 41]. In [42], the optimised PIM level of a circulator was -95 dBm at 1.2 GHz with $P_{\mathrm{Tx}} = 48$ dBm. However, it has been reported that the origin of PIM in ferrites is still not fully understood, because apparently identical devices exhibit large variations in their PIM signal level [43].

3.2.3 Dielectric materials

Only few measurement results on the PIM level of dielectric materials have been reported. The third order intermodulation level spread of four different dielectric resonator materials was 55 dB with a field strength of 10 V/mm at 800 MHz [44]. The sample of high-purity (Zr,Sn)TiO_4 had a distortion level of -85 dBm with $P_{\mathrm{Tx}} = 55$ dBm, which corresponded to the field intensity of 60 V/mm. The nonlinear permittivity was explained by the displacement of the ions in the lattice. High-quality alumina (99.7%) was found to generate a PIM signal in a PIM measurement setup whereas the use of PTFE (polytetrafluoroethylene) decreased the level to the system residual [18]. In later measurements with a similar measurement setup, the PIM levels of alumina and PTFE samples were below the residual level of -125 dBm, whereas the samples of polystyrene, polythene, and nylon 66 generated a PIM level from -102 to -112 dBm when exposed to the maximum field strength of 1000 V/mm at 1.5 GHz [39].

3.2.4 Other phenomena

As is the case with the a-spots in Sect. 3.1.2, the temperature dependency of conductivity causes PIM distortion in devices made of metal. It has been theoretically calculated that its effect can produce PIM levels from -140 to -130 dBm with $P_{\mathrm{Tx}} = 45$ dBm at 200 MHz in coaxial cables [45].

The volume change of dielectric materials with the electric field strength is called electrostriction [46]. It is present in every dielectric material and it causes the nonlinear behaviour of the permittivity. Kumar suggests that these effects could contribute to the PIM generation in coaxial cables but presents no measurement results [47]. Carbon fibre, which has been used in reflector antennas, can also produce considerable PIM levels [48].

The behaviour of the permittivity in ferroelectric materials is similar to that of the permeability in ferromagnetic materials [46]. Ferroelectric materials are insulators and thus can be used at microwave and millimeter wave frequencies. They have been used in devices such as varactors, tunable filters, phase shifters, mixers and parametric amplifiers [49]. For a ferroelectric capacitor, a third-order intermodulation level of -70 dBm was achieved with $P_{\mathrm{Tx}} = 15$ dBm at 1.9 GHz [50].

3.3 Surface effects

The abrasion or contamination on a conductor surface may also cause PIM distortion, if the current density is high enough. The surface effects have been studied at 1.5 GHz with an input power of 44 dBm in [18,39]. Test samples were 1 mm diameter metal wires made of aluminium,

aluminium alloy 6061, copper, and beryllium copper with different surface treatments. The samples acted as centre conductors of a coaxial cable with a current density of 225 A/m per carrier. In the surface roughness test the surface of the wires was abraded orthogonally to the current as well as longitudinally. The orthogonal abrasion resulted in an increase of 13 to 22 dB from the residual PIM level of -144 dBm, whereas the longitudinal abrasion had an effect of 1 to 4 dB. The oxidisation of copper and beryllium copper samples had no effect on the observed PIM level. The silver plating with thickness of 13 μm on the nickel wire resulted a decrease of 48 dB to the residual PIM level. The plating of aluminium and aluminium alloy 6061 with silver or Alocrom 1200 had no significant effect on the PIM level. It has been proposed that also the roughness of the copper foil on printed circuit boards could generate PIM distortion [51].

The leftover from solder flux can also produce PIM distortion. The author observed a decrease of the PIM level from -110 dBm to the residual PIM level of -120 dBm with $P_{\mathrm{Tx}} = 43$ dBm when the resin was cleaned away from the centre conductor junction of a microstrip to coaxial line transition.

3.4 Time dependency of PIM sources

In addition to the PIM level variation between apparently similar devices, the variation with regard to time is a typical characteristic of a PIM source [52]. The changes may happen in small or large time scale and especially loose metal contacts can produce random variation within seconds [53]. The changes can be gradual or abrupt as can be seen in PIM level measurements versus time in Fig. 6. In the first example, the PIM level is unstable almost all the measurement time until the device breaks down in the PIM sense. The PIM response of the other microstrip line seems to be relatively stable after warming up three hours. The probable PIM source in both devices was a metal contact in the connector.

The properties of the metal as well as a tarnish film or contamination on the metal surface change with the temperature and humidity or as they are exposed to various molecules and particles in the air. For example, the hardness of a metal changes with temperature and with time due to the thermal diffusion of atoms under the influence of stress [15]. Dust is usually hygroscopic and may be insulating or conducting depending on the humidity [54]. The corrosion of the metal contacts should naturally be avoided and it should be noted that the use of dissimilar metals in a contact increase the risk of corrosion. Also fritting may cause irreversible changes in a junction.

A relative movement of contact surfaces can cause the change, removal or appearance of a-spots. The movement can be caused by external vibration, thermal expansion or electromechanical force caused by large currents. When the contact surfaces rub against each other the mechanical movement wears the contact surfaces and extracts particles which corrode or oxidise easily. This phenomenon is called fretting corrosion and it causes typically an increase in the contact resistance and it may cause contact failure in electrical connectors. The amplitude of the movement in electrical connectors ranges typically from 1 to 100 μm whereas the frequency of the motion typically spans from very slow temperature variations to one hundred hertz due to mechanical vibration [55].

3.5 Coatings and soldering

Silver plated devices have been found to have good PIM properties [18, 56, 57]. Gold and some copper alloys are other materials that have been widely used in high-frequency coatings.

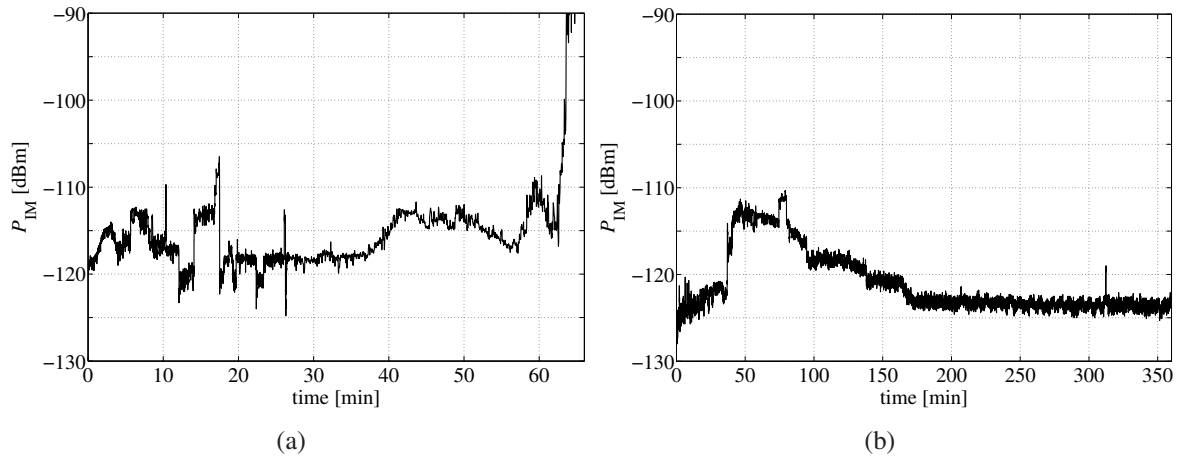

Figure 6. PIM level of two microstrip lines versus time: a) microstrip no. 1, b) microstrip no. 2.

Silver and gold have also been found to be more resistant to fretting than base metals and their alloys [55]. However, when nickel is used as a bonding layer between the matrix metal and the coating, there is a risk of getting high PIM levels when the outer layer is rubbed off. The effect of the contact pressure was studied on silver, gold and copper alloy plated junctions in [58]. It was concluded that all the platings performed well when the contact force was high enough. The required contact force was lowest for gold and highest for the copper alloy. The coatings made of titanium nitride, Alocrom 1200, and indium performed well in [59]. On the contrary, in [18] Alocrom 1200 plated junctions were found to produce highly variable PIM levels. Such discrepancies might be explained by the differences in the coating processes or in their quality. Finally, it is known that low PIM levels in metal contacts can be achieved by soldering [39].

4 General guidelines for the design of low-PIM devices

In this chapter, general guidelines are given for assisting the design of low-PIM devices. It is apparent, that usually it is not practical to follow them all at the same time, because the required PIM level, the intended use of the device, and the allowed manufacturing costs affect the device design. Also, some effects are much stronger than other. For example, ferrites generate much larger PIM levels than commonly used dielectric materials.

Typically, the PIM level is dependent on the current density, which should be minimised at the PIM source. Therefore, the potential PIM sources should be placed at the locations of current minima. However, these locations move with the frequency, which leads to the recommendation that the transmitting signals should be well-matched over the whole bandwidth of the device. Chapter 5 is devoted to the study of this loading impedance effect.

An apparent way to decrease the current density at a junction is to increase its contact area. However, it must be remembered that the conducting areas must be made larger; it is not sufficient to increase the apparent or load bearing area of the contact. In fact, a larger contact area might even increase the PIM level, because the contact pressure is lower and there are more potentially bad contact spots. A better approach is to have a well-defined contact area with precise mechanical dimensions.

The recommendations are mainly collected from Chapter 3 and from [60–62]. In addition to the component design, the PIM performance of a system can be optimised by frequency planning and by providing enough isolation between the transmitting and receiving signals.

Nonlinear materials:

- Do not use ferrites or ferroelectric materials since their PIM levels are usually unacceptably high.
- Avoid the use of ferromagnetic materials. If they have to be used, do not locate them in the vicinity of high field strengths. They can be plated with linear material, but then the thickness of the plating must be several skin depths and it must be taken care of that the cover material will not wear away in the use [18].
- Some dielectric materials can also be nonlinear as stated in section 3.2.3.

Metal-to-metal contacts:

- Avoid metal-to-metal contacts in the signal path, when possible. For example, a coaxial connector essentially without metal-to-metal contacts has been designed for the frequency band of 0.5–2.5 GHz [63].
- Avoid loose contacts and rotating joints in the vicinity of high field strengths. These include the tuning and mounting screws, bolts, and rivets. Consider the relocation of the contacts or using insulators between the metal surfaces.
- Use solders of good quality instead of mechanical contacts. Make sure that there will be no nonlinear materials or solder waste in the contact.
- Use adequate contact pressure. The required pressure depends also on the metal [58], but it should be noted that a high pressure alone is not sufficient for good PIM performance.
- Use metal coatings as described in section 3.5.

Metal surfaces, section 3.3.:

- The metal surfaces that are subject to high current densities should be especially clean and smooth.
- Do not use too thin conductors.

High-quality workmanship, assembly and maintenance:

- Use flat and smooth contact areas with precise mechanical tolerances.
- During and after the assembly, the metal contacts should be free of metal particles, contamination, and oxidisation.
- During the life-time of the device, protect the contacts from contamination, oxidisation, and corrosion.
- During the life-time of the device, minimise the relative movement of contact surfaces due to external vibration, thermal expansion, and electromechanical forces.

Coaxial cables:

- Avoid coaxial cables that have steel alloys in their centre conductor.
- Prefer coaxial cables with corrugated or rigid outer conductors. However, also other cables can perform well, such as the flexible semirigid cable Sucoform 141 and the braided RG 393 cable. However, Sucoform 141 has a tin-coated outer conductor, and therefore, should not be bended too many times, since microcracks could be formed in the outer conductor.
- Do not bend cables too much. Especially critical point is the base of the connector, where the contact between the connector and the outer conductor of the cable is located.

5 PIM source as a circuit element

As was stated in Chapter 3, there are no validated physical models for PIM sources. Typically a simple Taylor polynomial model has been used [29, 64–66], although it fails to explain the time and power dependency of a PIM source. The 3rd degree polynomial model predicts a cubic dependency of the third-order PIM power on the transmitting power, whereas in measurements the dependency has been found to vary from 1.6 to 3.0 dB/dB in different devices [33, 66, 68]. Various power slopes can also be seen in the antenna measurement results in Fig. 2. As a special case, the amplitudes of the intermodulation products generated by an exponential nonlinearity can also be evaluated directly with the help of modified Bessel functions [67].

The available power of a nonlinear circuit element at an intermodulation frequency is affected by the loading impedances at different frequencies. For example, the intermodulation distortion level of a microwave BJT (bipolar junction transistor) or FET (field effect transistor) power amplifier is affected by the impedance at the baseband frequencies [69, 70]. The baseband impedance may increase or decrease the IM levels or may cause asymmetry between the upper and lower IM levels. On the other hand, the efficiency of diode frequency multipliers can be improved by using so called idlers [8]. An idler is typically a resonator that creates a short circuit at a certain harmonic frequency, but has minor effect at the input or output frequencies. Recently, there has been speculations whether the idlers could be used in suppressing PIM distortion [71]. However, those results can be explained by the impedances at the fundamental frequencies.

The Taylor polynomial model approach is used in this thesis in order to investigate the effects of the loading impedances at the transmitting and intermodulation frequencies on PIM signals. The PIM source is assumed to be independent of time and to obey a third degree polynomial. Although the model could be considered naive, it can describe some of the characteristics that are found in PIM measurements. In [P3], the model was successfully used to explain the PIM signal dependency on the load impedance as well as on the frequency. The same model was used in [P4] to predict the differences in reverse and forward travelling PIM waves and to explain the PIM near-field measurement results. Also the addition of two PIM sources was considered.

5.1 PIM source model

PIM signals are usually considered as small signals in the analysis because they are more than 100 dB below the carrier power level. If the PIM source is assumed to be memoryless, the Taylor polynomial is a natural choice to model a PIM source.

Another popular small signal method is the Volterra series analysis, which can include the memory effects of the nonlinear device. It is implemented, for example, in modelling intermodulation behaviour of FET and BJT power amplifiers, where the nonlinear device has a known analytical model [69]. Also, the Taylor polynomial model can be extended to include memory effects. The use of complex coefficients represent time delays for different order nonlinearities and thereby the dependency of the phase shift on the power level can be taken into account [72]. The generalised power series analysis goes even further and takes into account also the frequency dependent amplitude and delay [73]. That is, the memory effects can also be incorporated to the model, and it has been shown that the Volterra series of a system can be found from its generalised power series expansion [74].

However, because the details of a PIM source are unknown, the memory effects cannot be taken into account and the Taylor polynomial is used. The PIM source is assumed to be in series with the signal path, but similar analysis can easily be done for a parallel PIM source, too. In order to keep the resulting equations simple, only the third degree term is taken from (2.1) to model the PIM source. The voltage across the source is

$$V_{\text{src}} = a_3 \left[I(f_1) + I(f_2) \right]^3, \tag{5.1}$$

where $I(f_1)$, $I(f_2)$ are the currents flowing through the PIM source at the frequencies of f_1 and f_2. a_3 is a real constant, that is, it does not depend on the frequency nor on the source and load impedances. This approximation implies that the voltage is a smooth function of the current and that the PIM source does not contain any reactive elements. Furthermore, the large and small signal resistances are assumed to be negligible compared with the source and load impedances Z_{s} and Z_{L}, respectively. The circuit model is shown in Fig. 7. The reflection coefficients seen by the PIM source are Γ_{s} and Γ_{L}.

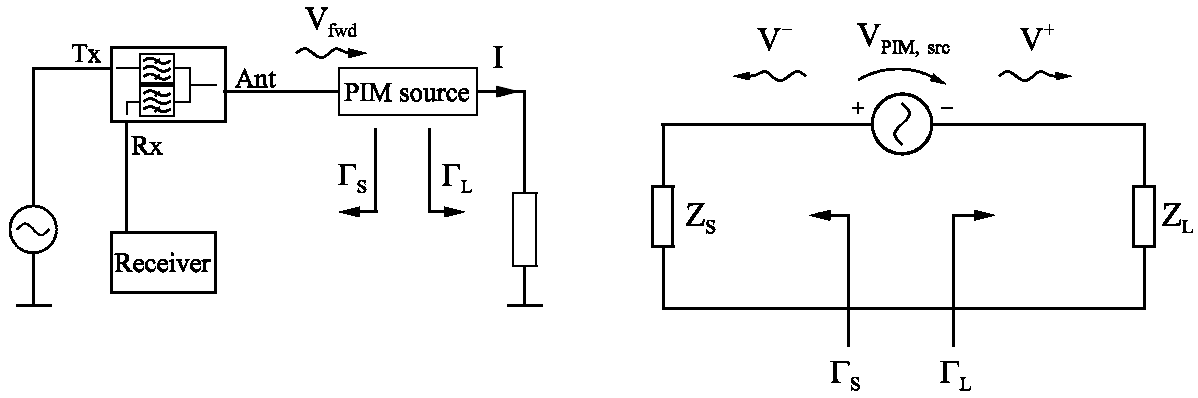

(a) Large signal model (b) Small signal model

Figure 7. Circuit model for the analysis of a serial PIM source.

The reverse and forward travelling voltage waves at the intermodulation frequency $f_3 = 2f_1 - f_2$ are

$$V^- = \frac{V_{\text{PIM,src}}}{2} \frac{1 - \Gamma_{\text{L}}(f_3)}{1 - \Gamma_{\text{s}}(f_3)\Gamma_{\text{L}}(f_3)}, \tag{5.2}$$

$$V^+ = -\frac{V_{\text{PIM,src}}}{2} \frac{1 - \Gamma_{\text{s}}(f_3)}{1 - \Gamma_{\text{s}}(f_3)\Gamma_{\text{L}}(f_3)}, \tag{5.3}$$

respectively. The voltage $V_{\text{PIM,src}}$ across the PIM source and the current at the transmitting frequencies are

$$V_{\text{PIM,src}} = \frac{3a_3}{4} I^2(f_1) I^*(f_2), \tag{5.4}$$

$$I(f) = \frac{V_{\text{fwd}}(f)}{Z_0} \frac{1 - \Gamma_{\text{L}}(f)}{1 - \Gamma_{\text{s}}(f)\Gamma_{\text{L}}(f)}, \tag{5.5}$$

where Z_0 is the reference impedance and the asterisk denotes the complex conjugate. The expression in (5.4) corresponds to the first term in (2.20). The reverse and forward PIM currents are

$$I^- = -\frac{V^-}{Z_0}, \tag{5.6}$$

$$I^+ = \frac{V^+}{Z_0}, \tag{5.7}$$

respectively.

5.2 Reverse and forward PIM power

The reverse and forward PIM powers of a single PIM source are

$$P_{\text{rev}} = \frac{|V^-|^2}{2Z_0}(1 - |\Gamma_{\text{s}}(f_3)|^2), \tag{5.8}$$

$$P_{\text{fwd}} = \frac{|V^+|^2}{2Z_0}(1 - |\Gamma_{\text{L}}(f_3)|^2). \tag{5.9}$$

It can be seen from (5.2)–(5.9) that the PIM power is proportional to $|1-\Gamma|^8$, when the reflection coefficients are assumed to equal constant Γ. If the load and source are perfectly matched, the reverse and forward powers will be equal

$$P_{\text{rev}} = P_{\text{fwd}} = \frac{9a_3^2}{16Z_0^4}P_{\text{av}}^3, \tag{5.10}$$

where P_{av} is the available power of the transmitter. Then, if the transmitted power is 43 dBm, $Z_0 = 50\,\Omega$ and $P_{\text{rev}} = -120$ dBm, the coefficient $a_3 = 1.2 \cdot 10^{-6}$ V/A^3. It is also seen, that with a serial PIM source the PIM level drops 12 dB when the system impedance is doubled. This can be utilised when designing the feeding networks of an antenna array.

The ratio of the reverse and forward PIM power is

$$\frac{P_{\text{rev}}}{P_{\text{fwd}}} = \left|\frac{1-\Gamma_{\text{L}}(f_3)}{1-\Gamma_{\text{s}}(f_3)}\right|^2 \cdot \frac{1-|\Gamma_{\text{s}}(f_3)|^2}{1-|\Gamma_{\text{L}}(f_3)|^2}. \tag{5.11}$$

5.3 Addition of multiple PIM sources

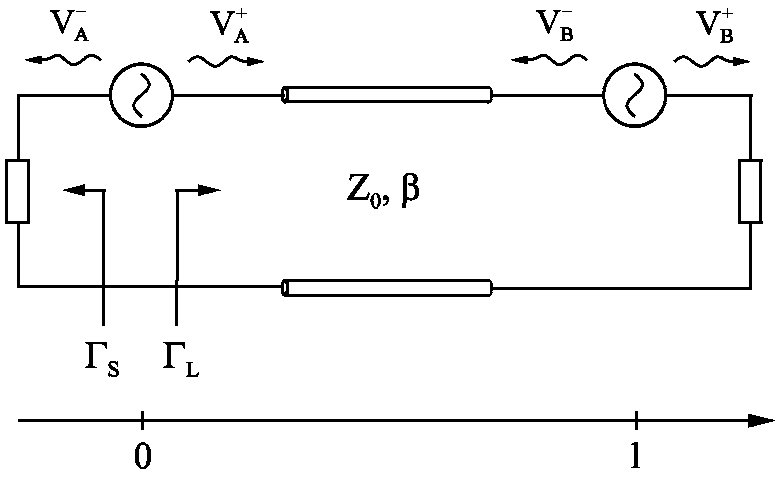

Figure 8. Two PIM sources separated by a transmission line.

There can be many PIM sources in the device, which may add up constructively or destructively. The magnitude of the sum voltage depends on the direction of the wave propagation, the electrical distance between the sources, and the reflection coefficients. There are two PIM sources separated by a transmission line of length l in Fig. 8. The sum of the forward travelling voltages V_{A}^{+} and V_{B}^{+} is

$$V_{\mathrm{AB}}^{+} = V_{\mathrm{A}}^{+} e^{-j\beta_3 l} + V_{\mathrm{B}}^{+}, \tag{5.12}$$

$$V_{\mathrm{A}}^{+} = rV_0 \frac{(1-\Gamma_{\mathrm{L},1})^2}{(1-\Gamma_{\mathrm{L},1}\Gamma_{\mathrm{s},1})^2} \frac{1-\Gamma_{\mathrm{L},2}^{*}}{1-\Gamma_{\mathrm{L},2}^{*}\Gamma_{\mathrm{s},2}^{*}} \frac{1-\Gamma_{\mathrm{s},3}}{1-\Gamma_{\mathrm{s},3}\Gamma_{\mathrm{L},3}}, \tag{5.13}$$

$$V_{\mathrm{B}}^{+} = V_0 e^{-j\beta_3 l} \frac{(1-\Gamma_{\mathrm{L},1} e^{j2\beta_1 l})^2}{(1-\Gamma_{\mathrm{L},1}\Gamma_{\mathrm{s},1})^2} \frac{1-\Gamma_{\mathrm{L},2}^{*} e^{-j2\beta_2 l}}{1-\Gamma_{\mathrm{L},2}^{*}\Gamma_{\mathrm{s},2}^{*}} \frac{1-\Gamma_{\mathrm{s},3} e^{-j2\beta_3 l}}{1-\Gamma_{\mathrm{s},3}\Gamma_{\mathrm{L},3}}, \tag{5.14}$$

$$V_0 = -\frac{3a_3}{8Z_0^3} V_{\mathrm{fwd},1}^2 V_{\mathrm{fwd},2}^{*}, \tag{5.15}$$

where r is the ratio of the coefficients a_3 of PIM sources A and B. β is the phase constant. The numbers in the subscripts refer to the frequencies f_1, f_2, and $f_3 = 2f_1 - f_2$.

The sum of the reverse travelling voltages is

$$V_{\mathrm{AB}}^{-} = V_{\mathrm{A}}^{-} + V_{\mathrm{B}}^{-} e^{-j\beta_3 l}, \tag{5.16}$$

V_{A}^{-} and V_{B}^{-} are obtained from (5.13) and (5.14) by substituting $\Gamma_{\mathrm{s},3}$ in the numerator with $\Gamma_{\mathrm{L},3}$.

If the load and source are perfectly matched the sum voltages reduce to the well known formulas

$$V_{\mathrm{AB}}^{+} = V_0 e^{-j\beta_3 l}(r+1), \tag{5.17}$$

$$V_{\mathrm{AB}}^{-} = V_0(r + e^{-j2\beta_3 l}). \tag{5.18}$$

It can be seen that the forward PIM waves add in-phase, whereas the reverse PIM waves may even cancel each other. Therefore, the forward PIM measurement seems to give the worst case performance of a device with multiple PIM sources. If the reverse PIM measurement is used, it has to be performed over the whole operating bandwidth of the device so that the possible minimum can be detected.

In practise, the situation is not so simple due to the source and load impedances. It may happen that the reverse PIM level is higher than the forward level when the distance between the PIM sources is about half wavelength. In that case the difference is typically small and the forward PIM level can still be considered as a worst case measurement. However, the effect of the loading impedances is clearly seen in the ratio of the PIM voltage caused by one and two PIM sources. The ratios $V_{\mathrm{AB}}^{+}/V_{\mathrm{A}}^{+}$ and $V_{\mathrm{AB}}^{-}/V_{\mathrm{A}}^{-}$ of two equal PIM sources calculated from (5.12)–(5.16) are plotted in Fig. 9. The source and load reflection coefficients were measured from a PIM equipment and an antenna, respectively. It is seen that on the contrary to (5.17), the sum of the forward travelling voltages depends on the electrical distance between the sources and it deviates from 6 dB. In the case of the reverse PIM, the cancelling of the waves is not perfect anymore.

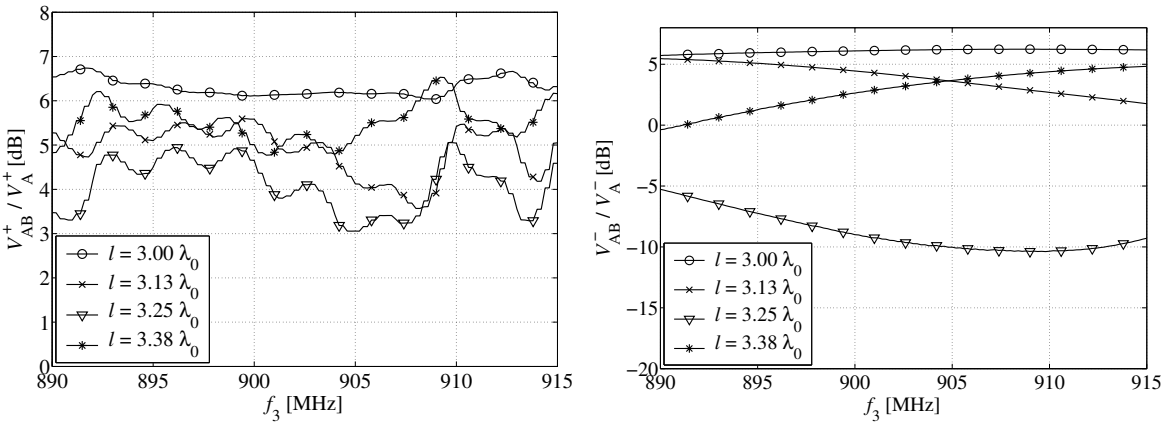

(a) Forward travelling wave

(b) Reverse travelling wave

Figure 9. Ratio of the PIM voltages caused by two and one PIM sources. Calculated from (5.12)–(5.16) with measured reflection coefficients $|\Gamma_s|, |\Gamma_L| < 0.2$. $f_1 = 925$ MHz, $f_2 = 935$–960 MHz, $r = 1$. λ_0 is the wavelength in the transmission line at $f_3 = 902.5$ MHz.

6 Localisation of passive intermodulation sources

6.1 Passive intermodulation measurements

Passive intermodulation signal measurements require specialised equipment so that the desired residual intermodulation level of the system can be achieved. Especially critical components are the power combiner and the duplex filter, which separates the transmitted and received signals. A block diagram of a typical PIM measurement system that can be used to measure both the forward and reverse PIM levels travelling PIM signals is shown in Fig. 10. Here, the terms reverse and forward are related to the direction of the high-power signal propagation. Two high-power signals are fed to the device under test (DUT) through Port 1. In the reverse PIM measurement mode, the RF switch is in position 'Rev' and in the forward measurement mode, the RF switch is in position 'Fwd'. The forward PIM measurement is sometimes favoured when measuring devices with two or more ports, since the method typically gives the worst-case performance of a device which contains several PIM sources.

The performance of a GSM base station antenna is usually evaluated as a reverse PIM measurement, which corresponds to the real operating conditions and is easier to establish than the forward PIM measurement. Provided that the frequency span is wide enough, the existence of multiple PIM sources in the device under test can be revealed when the reverse PIM level is measured as a function of frequency. For example, in the GSM 900 frequency band the distance between the PIM sources in a cable must be a few meters to be reliably discovered. The measurement must also last long enough so that the possible time dependency of the PIM level can be obtained. In addition, environmental tests can be applied before or during the PIM measurement, since minor changes in the metal contacts can affect the PIM level as was discussed in Sect. 3.4. Because PIM level of a device is perhaps the most sensitive indicator of a nonlinearity, the PIM measurement can also serve as an indicator of the device quality.

6.2 Localisation methods

PIM sources have been located by different means depending on the type and size of the component or structure to be studied. The simplest method is the trial and error procedure where one first tries to recognise the likely distortion sources by visual inspection. Then the PIM level is monitored simultaneously as the source candidates are tapped or cooled down with a cold spray. If this method does not lead to results, the suspected parts can be replaced until the PIM level decreases down to an acceptable level. Although this approach is straightforward, it is often very time consuming and sometimes the replacement is not possible.

When the PIM sources are located in the antenna structures or objects nearby, a receiver with a directional antenna can be used. PIM sources on naval ships were localised with a ferrite rod antenna at 1 to 5 MHz [31].

In order to find the strongest PIM source, the PIM signal at the frequency of the maximum order was selected from the many PIM signals present. Small loop antennas were tested in detecting the PIM sources in radio towers, but the low directivity of the antenna hindered the exact localisation of the sources [68]. The problems found in the field tests were the standing waves, self-generated PIM of the receiving antenna and detector, as well as the reradiation of the PIM signals from resonant structures.

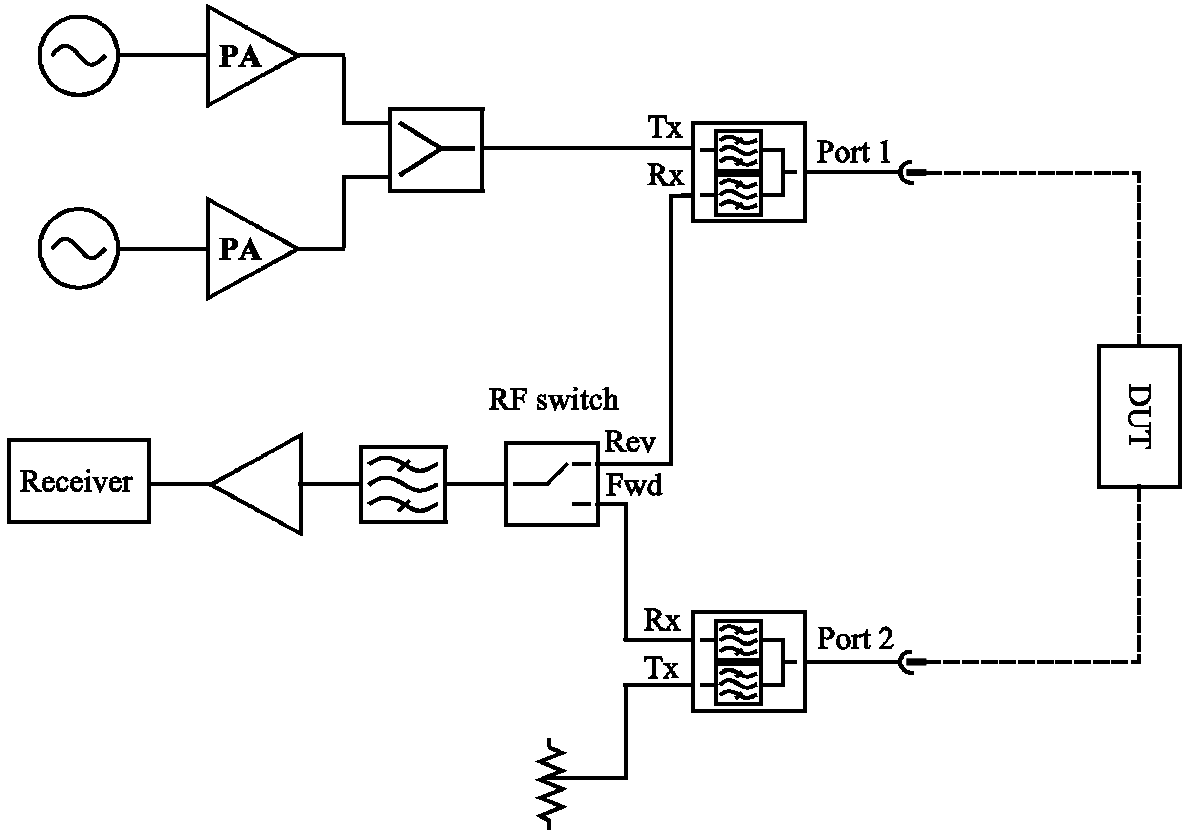

Figure 10. Block diagram of a typical PIM measurement equipment.

The measurement equipment can also contain both the transmitters and the receiver. Two transmitting antennas illuminate the suspected structure while the PIM signal is received by a directive antenna. Such a technique was used to scan the walls of an anechoic chamber at 1.5 GHz [75]. Microwave holography was applied to locate PIM sources in reflector antennas at 8 GHz [76]. The reflector was illuminated with two transmitting feed horns and the scattered field was sampled in the radiating near field with a planar scanner at the intermodulation frequency. The field distribution in the aperture of the reflector was then calculated with the holographic technique [77]. The main problems in this measurement were the self-generated PIM of the transmitting and receiving antennas as well as the required high dynamic range of the system.

A cable radar principle was applied in order to detect PIM sources in microwave link antenna cables at 11 GHz [78]. The two carriers were modulated with 2 ns pulses while the reverse PIM pulses were detected at the intermodulation frequency. The resulting distance resolution was approximately 0.8 m but the sensitivity was considerably less than that of the corresponding CW system.

6.3 Near-field scanner

A passive intermodulation near-field measurement method has been developed within this thesis work. The method can be used to localise PIM sources in open devices and structures such as microstrip lines and antennas. The block diagram of the scanner and the details of the reference signal unit are shown in Fig. 11 and Fig. 12, respectively. The idea is to scan the field strength of

the device under test (DUT) with a near-field probe at the intermodulation frequency. The probe is at a distance of less than tenth of a wavelength from the DUT so that good sensitivity and high spatial resolution are achieved. The scanner has been realised in the GSM 900 frequency band with the capability to detect the amplitude and phase of the third-order PIM signal. The phase information helps to localise the PIM sources and lowers the system noise floor. The maximum scanning area is 0.3×1.0 m^2. The scanner has been used to localise PIM sources with reverse PIM levels from -111 to -80 dBm ($P_{\mathrm{Tx}} = 2 \times 43$ dBm) in antennas and microstrip lines. The main limitation of the scanner is the self-generated PIM distortion in the near-field probe, which may lower the sensitivity of the scanner when the probe is close to the metal edges of the DUT. This degradation of the sensitivity depends both on the probe and on the structure of the DUT.

The concept of the scanner was introduced in [79] and the scanner sensitivity was analysed in [P2, 80]. Description of the scanner as well as demonstration measurements of PIM sources in a two-element antenna array and on a microstrip line were presented in [P1]. Further measurements of various PIM sources on microstrip lines were shown in [P4, 81].

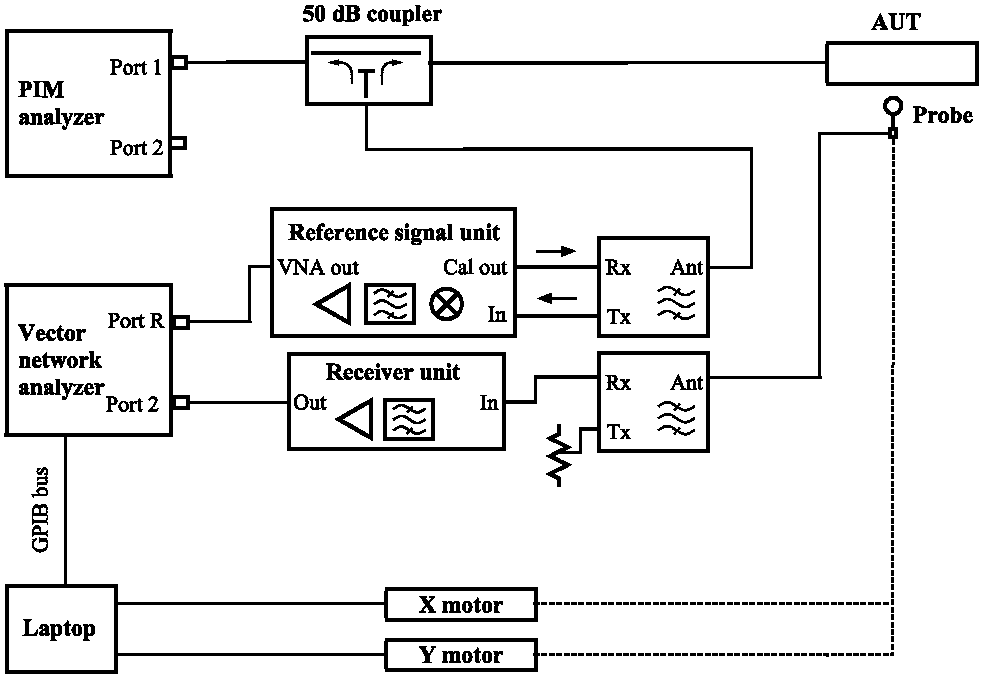

Figure 11. Block diagram of the PIM near-field scanner.

6.3.1 Low-PIM components

This section describes the low-PIM components that have been used in the near-field scanner or in the test measurements.

A commercial PIM analyser SI-900E by Summitek Instruments is used as the high-power signal generator and combiner. The instrument is also used to measure the reverse PIM level. Cellflex SCF12-50 corrugated cables and braided RG 393 cables with 7/16 type connectors has been used in the PIM measurements. The components that are not commercially available – the near-field probes, the 50 dB coupler, the test antenna, the test microstrips, and the variable load – are self-made. The design of the near-field probes is described in section II B of [P1].

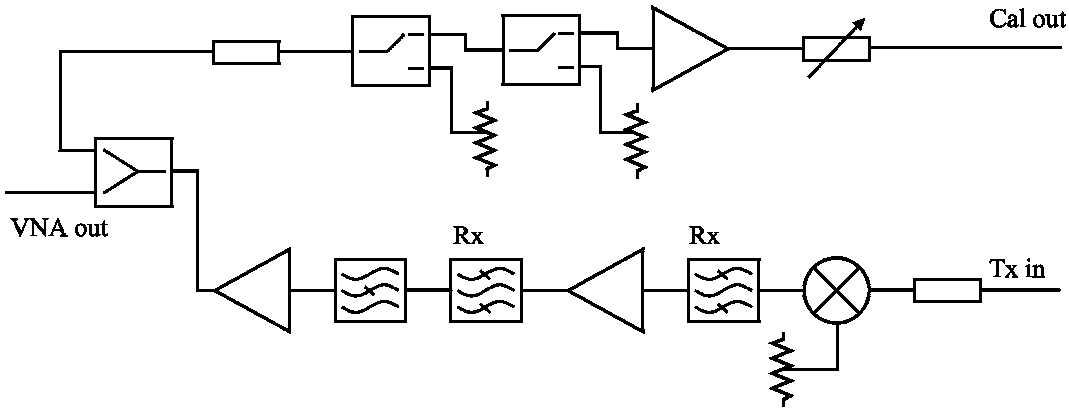

Figure 12. Block diagram of the reference signal unit.

The 50 dB low-PIM coupler in Fig. 11 can be replaced with three normal couplers provided that there is access to the transmitting and receiving signals before they are combined. Because this was not possible with the PIM analyser, a self-made low-PIM coupler has been designed and constructed. The design of the coupler is shown in Fig. 13. Part of the outer conductor of the Sucoform 141 cable is milled away and a circular plate probe is placed in its vicinity. The structure is mounted in a small brass block so that the radiation is suppressed. The measured S-parameters are $S_{11}, S_{22} < -35$ dB, $S_{21} > -0.05$ dB and $S_{31}, S_{32} = -47.5$ dB in the frequency range of 890–960 MHz. The measured reverse PIM level is less than -120 dBm with the transmitting power of 2×43.75 dBm and the PIM frequencies of 890–915 MHz.

The low-PIM test antenna, which has been used in [P1] and [P2], is a microstrip-fed stacked patch antenna. It has an N type connector attached to the silver-plated aluminium ground plane. The lower patch is etched on a 1.6 mm thick Rogers RTDuroid5880 substrate is and the upper patch is on a 1 mm thick FR4 substrate. Nylon screws and bakelite posts are used to support the upper patch. The copper has been removed from the ground plane side of the Duroid substrate, so that the ground plane current flows in the silver plating. Nylon screws are used to attach the lower substrate to the ground plane. The return loss of the antenna is more than 14 dB, when $f = 890 - 960$ MHz and the measured reverse PIM level is less than -118 dBm with the transmitting power of 2×43 dBm and the PIM frequencies of 890–915 MHz.

The test microstrip lines have a milled aluminium ground plane and 7/16 connectors attached to it. The strips are made from tin-copper sheet. In some microstrip lines, Rohacell HF51 foam is used as a substrate, and in other cases no substrate was used.

The variable load, which was used in the measurements of [P3], is based on the microstrip line. It has a 5 mm thick triangular PTFE slab, which can be slid under the microstrip. The slab has milled quarter-wavelength sections in order to improve the impedance matching. The return loss depends on the slab position, but is always better than 13 dB, when $f = 890 - 960$ MHz. The measured reverse PIM levels of the microstrip lines and of the variable load are less than -117 dBm with the transmitting power of 2×43 dBm and the PIM frequencies of 890–915 MHz.

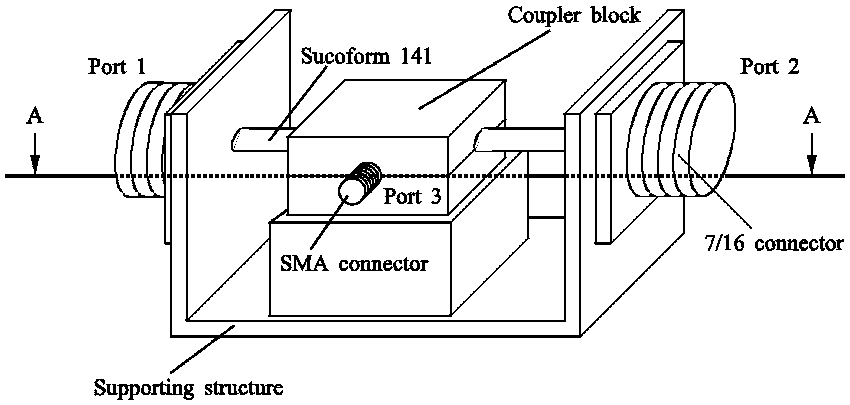

(a) Sketch of the 50 dB coupler.

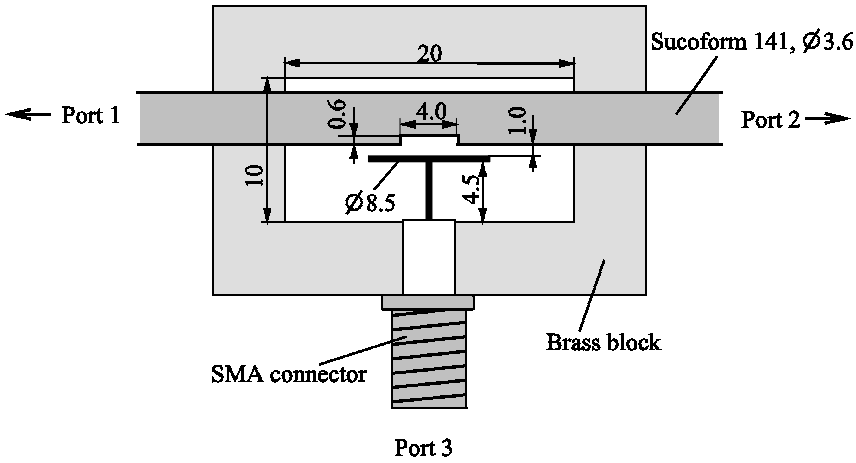

(b) Dimensions of the coupler block. Cut A-A.

Figure 13. Design of the 50 dB coupler.

7 Broadband dual-polarised microstrip antenna elements for antenna arrays

Many different kinds of antenna elements have been used in moderate bandwidth (10–20 %) array antennas. These include horn antennas, slotted waveguides, dipoles, and dielectric antennas [82, 83]. Also antennas etched on a printed circuit board, such as patch antennas, printed dipoles and slot antennas, have received considerable attention. Many dual-polarised antenna elements have been designed for various applications and frequency bands. Especially numerous are the designs based on microstrip techniques [84–90]. Microstrip antennas enable the mounting of integrated circuits on the antenna, they have low profile, are lightweight, and are easy to fabricate.

7.1 Compact antenna element

In order to fit in an array antenna and to avoid grating lobes, the size of the antenna element must not exceed half of the free-space wavelength. Besides the radiating part also the feed of the antenna has to be as compact as possible. The requirements for regular radiation patterns and low cross-polarisation level typically imply that the geometry of the antenna element and its feed have to posses symmetry. The more severe are the requirements the more symmetrical the antenna element has to be.

A single patch antenna can be thought as a resonator, whose impedance bandwidth depends on its unloaded quality factor Q_0. The optimally coupled resonator has a relative bandwidth of [91]

$$\frac{\Delta f}{f_0} = \frac{1}{Q_0}\frac{S^2-1}{2S}, \tag{7.1}$$

where f_0 is the resonant frequency and S is the maximum voltage standing wave ratio over the bandwidth. It is known that the bandwidth of electrically small antennas can be improved by increasing the volume of the antenna. The same applies to microstrip antennas. The quality factor of a patch antenna decreases when the substrate thickness or the patch width is increased, or when the permittivity of the substrate is decreased. Therefore, thick, low-permittivity substrates are preferred in the microstrip antenna design. The use of a low-permittivity substrate also decreases the risk of surface wave generation, which degrades the radiation performance of the antenna and may lead to scan blindness in phased array antennas [92].

The bandwidth of a resonator can be increased with a lossless matching circuit. The maximum theoretical upper bound for the relative bandwidth is then $k_B \Delta f / f_0$, where the bandwidth-enlargement factor is [91]

$$k_B = \frac{2\pi S}{(S^2-1)\ln[(S+1)/(S-1)]}. \tag{7.2}$$

The matching circuit can be realised with lumped or distributed elements or it can be incorporated within the antenna structure by using parasitic patches [85]. Also the feed of the antenna can be used as a matching circuit. The slot in the aperture-coupled antenna or the combination of the probe and capacitive feed can be used as a matching element [93, 94].

Besides the impedance matching, also the radiation properties such as pattern symmetry, sidelobe level, and cross-polarisation level must remain within the requirements over the whole

bandwidth. Especially in many small antenna designs the wide impedance bandwidth has been achieved by utilising multiple radiation modes or complicated geometries, which deteriorate the radiation performance. As such these designs are not suitable for array antenna applications.

7.2 Antenna feed

The feed of a patch antenna can be implemented by a direct coupling with a microstrip line or a probe, by a capacitive coupling, or by an aperture coupling. The aperture-coupled microstrip antenna has received considerable attention since it was introduced in [95]. It allows different substrates to be used for the feeding network and the antenna element. Because the feed and the radiating element are located on different sides of the ground plane, low sidelobe (35 dB) and cross-polarisation levels can be achieved [96]. In addition, the antenna can be fabricated without vias, which lowers the manufacturing costs. On the other hand, the aperture in the ground plane radiates also backwards. Therefore, a metal plate is typically used behind the aperture-coupled antenna. In some cases, the back plate increases mutual coupling between the elements so that cavities are needed behind the elements in order to suppress the coupling [82, 86].

Prior to the choice of the feeding line substrate, considerations on losses, undesired radiation, cross coupling, manufacturing tolerances, available space, and possible integration of passive or active circuits must be done.

7.3 Antenna elements for 12 GHz array antenna

In this work, two dual-polarised microstrip antenna element types were designed for phased array antenna applications in the 12 GHz frequency band [P5, P6]. The design goals for the azimuthal and elevation scanning angles were $\pm 30^\circ$ and $\pm 3^\circ$, respectively. Therefore, the antenna elements were tested in subarray configurations of 4x1 elements.

Symmetric half-wavelength patches were selected as the basic shapes for the antenna elements so that reasonably symmetric and similar radiation patterns are achieved for both polarisations. However, the feed structures are asymmetric, because full symmetry requires the use of power dividers for each element [86, 97], which increases the needed circuit board space. The elements utilise dual-resonant structure in order to achieve an impedance bandwidth of 16 %. The element in [P5] is a three-layer structure with a resonant aperture and a single square patch. In [P6], there are four substrate layers so that the feed lines can be separated into two layers. The dual-resonance is achieved with a stacked patch configuration. Both the aperture coupling and the direct microstrip line feed are used in the designs. In both designs, the one port is fed at the centre of the antenna element and the other port at the edge so that the isolation between the ports is better than 35 dB.

8 Summary of publications

In paper [P1], the principle of the passive intermodulation near-field measurement method is described and the constructed equipment as well as measurement results are presented. The passive intermodulation scanner works at the GSM 900 frequency band and is capable of delivering two 43 dBm signals to the device under test. The concept of the normalised PIM level is presented, which helps to compare the scanning results with the reverse PIM measurement and to distinguish a PIM source in a device where the field distribution is not uniform. Also the sensitivity issues are considered based on the results presented in [P2]. A two-element dipole array and a microstrip line are used as test objects with reverse PIM levels from -108 dBm to -87 dBm. The defective antenna element is recognised from the scanning results, but not the exact location of the PIM source. In the microstrip, the location of the source is clearly seen both in the amplitude as well as in the phase data. The usefulness of the PIM phase data is demonstrated by a measurement, where the PIM source is located outside the scanning area. In the results the amplitude is constant along the microstrip line, but the PIM phase shows the direction where the PIM source is located.

Paper [P2] deals with the various factors that limit the PIM scanner sensitivity. The causes of residual intermodulation distortion are divided into internal and external sources and then analysed separately when possible. The near-field probe, the probe cable, and the receiver are the internal sources and the anechoic chamber, linear guides, and other metallic objects in the chamber are accounted as the external sources. The measured thermal noise level of the receiver is -172 dBm/Hz and the cable leakage is negligible. The chamber without the scanner is tested with a low-PIM antenna, whereas the PIM level caused by the chamber including the scanner is presented in [P1]. The total scanner sensitivity is investigated with low-PIM test object measurements, in which the residual PIM level remains mostly below -117 dBm and -115 dBm over the test object area with electric and magnetic field probes, respectively. It is also reported that the PIM level of the system tends to decrease or increase near the metal edges of the test object. It is supposed that this distortion is caused by other field components than the field component that is to be measured. Thus, the most critical part of the scanner is found to be the implementation of the near-field probes. Thermal noise and background PIM caused by the external sources limit the sensitivity further away from the test objects. It is concluded that the scanner is capable of detecting PIM sources down to -110 dBm with a transmitted power of 2×43 dBm and that the optimum coupling from the device under test to the probe is between 30 and 40 dB. However, the PIM distortion level of the near-field probe decreases the sensitivity of the scanner when the probe is located near the metal edges of the device under test. Therefore, the use of both electric and magnetic field probes can be helpful in the interpretation of the scanning results.

Paper [P3] presents the effect of the loading impedances on the PIM level measurements. Closed-form formulas are suggested for the reverse and forward PIM level dependency on the load and source impedance. The nonlinearity of the PIM source is assumed to obey the third-order Taylor polynomial model. The validity of the formula is tested by measuring the PIM power of a PIM source with 50 different load impedances, whose reflection coefficients varies between 0 and 0.3. The measured and calculated results show good agreement with the mean and maximum difference of 0.9 dB and 4.3 dB, respectively. It is found out that the measured PIM level is strongly dependent on the reflection coefficient of the load. If the load reflection coefficient were frequency independent, the magnitude of the reverse PIM level variation would be proportional to the eight power of the voltage standing wave ratio.

Paper [P4] utilises the model introduced in paper [P3] in order to explain the behaviour of PIM near-field scanning results. Equations for the PIM voltage along a transmission line are given. The effect of the loading impedances is considered and it is found out that the difference between the reverse and forward travelling PIM waves can be typically a few decibels. The addition of the voltages from two PIM sources is discussed and it is concluded that the sum depends clearly on the loading impedances. In general, forward travelling voltage waves do not add fully in-phase. The theoretical PIM signal characteristics are compared with the near-field measurement results of PIM sources in a microstrip line.

In [P5], a dual-polarised microstrip antenna element with high isolation is presented. The wide bandwidth is achieved by using a resonating coupling slot together with a thick, low-permittivity substrate. The high isolation results from the proper positioning of the coupling slots and from the thin substrate of the feeding network. One slot is on the edge of the patch whereas the other is offset sidewise from the middle. The return loss and the isolation between the input ports of the antenna element are better than 10 dB and 40 dB over the frequency range of 10.70 to 12.75 GHz. The maximum cross-polarisation level of the four-element array within the 3 dB beamwidth is -20 dB over the frequency band.

Paper [P6] presents a broadband dual-polarised microstrip element where the feeding networks for different polarisations are distributed on separate layers. Aperture coupling is utilised both in the feed of the element as well as in the transition from one layer to another. The return loss and the isolation between the input ports of the antenna element are better than 10 dB and 35 dB over the frequency range of 10.7 to 12.6 GHz. The maximum cross-polarisation level of a four-element array within the 3 dB beamwidth is -26 dB and -17 dB for ports 1 and 2, respectively. The estimated radiation efficiency of the array is 60–70% and 50–60% for ports 1 and 2. The lower efficiency of port 2 is due to the insertion loss of the aperture-coupled transition.

9 Conclusions

A passive intermodulation near-field measurement method was developed and load impedance effects on passive intermodulation measurements were studied in this thesis. In addition, new microstrip antenna elements that can be used in dual-polarised phased-array antennas were designed.

The localisation of the PIM sources in antenna structures was considered as an important topic in the design and fabrication of base station antennas. Therefore, a near-field measurement equipment in the GSM 900 frequency band was designed, constructed and its performance verified. The implementation of the scanner was found to be relatively straightforward to an existing PIM equipment. The scanner is capable of locating PIM sources in antennas and in other open structures, whose PIM level can be as low as -110 dBm with the transmitted power of 43 dBm. It was found out that the self-generated PIM distortion of the near-field probe is the main limiting factor of the scanner sensitivity. This distortion is typically highest near the metal edges of the device under test and may degrade the PIM scanner sensitivity. It was also concluded that the PIM distortion of the probe depends not only on the probe but also on the structure of the DUT. A clear difference between the performance of various probes was observed. The author believes that their performance can still be improved by a proper choice of the structure and materials, by a careful fabrication, and by applying some coating on the probe.

The effect of the source and load impedances on the PIM measurements was studied by treating the PIM source as a serial voltage source with negligible impedance. Many simplifying assumptions were made in the model, but the measurement results support the theory. The measurements were carried out by using an N–N-adapter as a stable PIM source and the mean difference between the calculations and the measurements was 0.9 dB. It is clear that the results cannot be applied for a time-dependent PIM source. However, the model is meant to be used in the design phase where a stable PIM response of the device has already been achieved.

The presented model was tested only with a single PIM source, so that more experiments are required in order to verify its validity. For example, it is often the case that the third-order PIM power dependency on the input power is not cubic, so that the used third-degree model is not valid anymore. In that case the presented results must be taken qualitatively. However, higher-degree terms can be incorporated in the analysis, if needed.

The treatment of multiple PIM sources in section 5.3 reveals that the forward PIM measurement does not give strictly the worst case performance of a device. Also, when taking the load impedance into account, the forward PIM level depends on the electrical distance between the sources. These statements differ from the common assumption how the forward PIM level behaves. Therefore, they will require more thorough theoretical and experimental investigations in future.

Because the effect of the load impedance on PIM measurements can be several decibels, it should be taken into account when considering the measurement accuracy of a PIM measurement equipment. The model has also implications in PIM testing of individual components of a system. There will be discrepancy in the performance of the device, when the final operating conditions differ from the test conditions. For example, if the PIM level of a two-port device is measured with a well-matched termination but finally connected with an antenna, the reverse PIM level will be different, in general. In the antenna design, the model can be used to explain and to predict the behaviour of a PIM source with changing environment. As an example, if

the connector is the major PIM source in an antenna and then the antenna is modified, also the measured PIM level can change although the PIM source remains the same.

There are a number of applications that utilise dual-polarised antennas. The contribution of the author has been to combine existing techniques in the design of antenna elements that can be used in phased array antennas with potentially low manufacturing costs. The elements use a dual-resonant structure in order to achieve a moderate impedance bandwidth (16 % with $L_{\mathrm{retn}} > 10$ dB). High isolation (35 dB) between the ports is gained by coupling one port at the electric and the other at the magnetic field maximum of the patch. The maximum cross-polarisation levels within the 3 dB beamwidth are between -17 and -26 dB. The elements are of compact size in the sense that no separate impedance matching circuit is needed in the feed. The antenna elements were designed for the European satellite television frequency band 10.70–12.75 GHz, but they are of course applicable at other frequencies, too. It should also be noted, that aperture-coupled antenna elements are suitable for base station antennas [86]. In addition to other properties, these elements are potentially low-PIM devices due to the lack of galvanic contacts in the feed.

References

[1] V. Golikov, S. Hienonen, and P. Vainikainen, "Passive intermodulation distortion measurements in mobile communication antennas," in *Proceedings of the IEEE VTS Vehicular Technology Conference VTC2001-Fall*, vol. 4, Atlantic City, Oct. 7–11, 2001, pp. 2623–2625.

[2] D. E. Foster, "A new form of interference – external cross modulation," *RCA Review*, vol. 1, Apr. 1937, pp. 18–25.

[3] P. L. Lui, "Passive intermodulation interference in communication systems," *Electronics and Communication Engineering Journal*, vol. 2, no. 3, June 1990, pp. 109–118.

[4] J.-G. Dumoulin, "Passive intermodulation and its effect on space programs," in *IEE Colloquium on Screening Effectiveness Measurements (Ref. No. 1998/452)*, London, May 6, 1998, pp. 2/1–2/10.

[5] K. Y. Eng and T. E. Stern, "The order-and-type prediction problem arising from passive intermodulation interference in communications satellites," *IEEE Transactions on Communications*, vol. 29, no. 5, May 1981, pp. 549–555.

[6] J. Boyhan, H. E. Lenzig, and C. Koduru, "Satellite passive intermodulation: systems considerations," *IEEE Transactions on Aerospace and Electronic Systems*, vol. 32, no. 3, July 1996, pp. 1058–1064.

[7] R. Singh and E. Hunsaker, "Systems methodology for PIM mitigation of communications satellites," in *Proceedings of the 4th International Workshop on Multipactor, Corona and Passive Intermodulation in Space RF Hardware (MULCOPIM2003)*, ESTEC, Noordwijk, Netherlands, Sept. 8–11, 2003, CD-ROM.

[8] S. A. Maas, *Nonlinear Microwave Circuits*. Piscataway, NJ: IEEE Press, 1997, 478 p.

[9] J. J. Bussgang, L. Ehrman, and J. W. Graham, "Analysis of nonlinear systems with multiple inputs," *Proceedings of the IEEE*, vol. 62, no. 8, Aug. 1974, pp. 1088–1119.

[10] R. A. Kishek, Y. Y. Lau, L. K. Ang, A. Valfells, and R. M. Gilgenbach, "Multipactor discharge on metals and dielectrics: historical review and recent theories," *Physics of Plasmas*, vol. 5, no. 5, May 1998, pp. 2120–2126.

[11] W.-C. Tang and C. M. Kudsia, "Multipactor breakdown and passive intermodulation in microwave equipment for satellite applications," in *Proceedings of the IEEE Military Communications Conference 1990 (MILCOM'90)*, vol. 1, Monterey, CA, Sept. 30–Oct 3, 1990, pp. 181–187.

[12] N. Rozario, H. F. Lenzing, K. F. Reardon, M. S. Zarro, and C. G. Baran, "Investigation of Telstar 4 spacecraft Ku-band and C-band antenna components for multipactor breakdown," *IEEE Transactions on Microwave Theory and Techniques*, vol. 42, no. 4, Apr. 1994, pp. 558–564.

[13] D. Wolk, J. Damaschke, C. Vicente, B. Mottet, H. L. Hartnagel, L. Galán, I. Montero, E. Roman, M. Alfonseca, J. de Lara, and D. Raboso, "AO-4025 ITT ESA – surface treatment and coating for the reduction of multipactor and passive intermodulation (PIM) effects in RF components," in *Proceedings of the 4th International Workshop on Multipactor, Corona and Passive Intermodulation in Space RF Hardware (MULCOPIM2003)*, ESTEC, Noordwijk, Netherlands, Sept. 8–11, 2003, CD-ROM.

[14] J. Puech, D. Belot, L. Baudenon, D. Gervaud, J.-R. Meyer, D. Faye, and J. Wyrwinski, "Corona effect on an antenna: start of the discharge, measurements of the impact on the RF transmission, comparisons with the theory," in *Proceedings of the 4th International Workshop on Multipactor, Corona and Passive Intermodulation in Space RF Hardware (MULCOPIM2003)*, ESTEC, Noordwijk, Netherlands, Sept. 8–11, 2003, CD-ROM.

[15] R. Holm, *Electric Contacts*, 4th ed. Berlin: Springer-Verlag, 1967, 482 p.

[16] G. C. Bailey and A. C. Ehrlich, "A study of RF nonlinearities in nickel," *Journal of Applied Physics*, vol. 50, no. 1, Jan. 1979, pp. 453–461.

[17] Y.-S. Wu, W. H. Ku, and J. E. Erickson, "A study of nonlinearities and intermodulation characteristics of 3-port distributed circulators," *IEEE Transactions on Microwave Theory and Techniques*, vol. 24, no. 2, Feb. 1976, pp. 69–77.

[18] J. S. Petit and A. D. Rawlins, "The impact of passive intermodulation on specifying and characterising components," in *Proceedings of the 3rd ESA Electronic Components Conference (ESA SP-395)*, ESTEC, Noordwijk, Netherlands, Apr. 22–25, 1997, pp. 45–49.

[19] A. P. Foord and A. D. Rawlins, "A study of passive intermodulation interference in space RF hardware," University of Kent at Canterbury," ESTEC contract 111036 final report, 1992.

[20] M. Runde, H. Kongsjorden, J. Kulsetås, and B. Tøtdal, "Detection of a-spots in aluminum contacts," *IEEE Transactions on Components, Hybrids and Manufacturing Technology*, vol. 9, no. 1, Mar. 1986, pp. 77–85.

[21] M. Runde, E. Hodne, and B. Tøtdal, "Experimental study of the conducting spots in aluminium contact interfaces," *IEEE Transactions on Components, Hybrids and Manufacturing Technology*, vol. 13, no. 4, Dec. 1990, pp. 1068–1073.

[22] R. D. Malucci, "High frequency considerations for multi-point contact interfaces," in *Proceedings of the 47th IEEE Holm Conference on Electrical Contacts*, Montreal, Canada, Sept. 10–12, 2001, pp. 175–185.

[23] J. D. Lavers and R. S. Timsit, "Constriction resistance at high signal frequencies," *IEEE Transactions on Components and Packaging Technologies*, vol. 25, no. 3, Sept. 2002, pp. 446–452.

[24] S. Selleri, P. Bolli, and G. Pelosi, "A time-domain physical optics heuristic approach to passive intermodulation scattering," *IEEE Transactions on Electromagnetic Compatibility*, vol. 43, no. 2, May 2001, pp. 203–209.

[25] M. Runde, "Mass transport in stationary contact points," *IEEE Transactions on Components, Hybrids and Manufacturing Technology*, vol. 10, no. 1, Mar. 1987, pp. 89–99.

[26] B. D. Jensen, K. Saitou, J. L. Volakis, and K. Kurabayashi, "Fully integrated electrothermal multidomain modeling of RF MEMS switches," *IEEE Microwave and Wireless Components Letters*, vol. 13, no. 9, Sept. 2003, pp. 364–366.

[27] W. H. Higa, "Spurious signals generated by electron tunneling on large reflector antennas," *Proceedings of the IEEE*, vol. 63, no. 2, Feb. 1975, pp. 306–313.

[28] C. S. Guenzer, "Comments on "Spurious signals generated by electron tunneling on large reflector antennas"," *Proceedings of the IEEE*, vol. 64, no. 2, Feb. 1976, p. 283.

[29] C. D. Bond, C. S. Guenzer, and C. A. Carosella, "Intermodulation generation by electron tunneling through aluminum-oxide films," *Proceedings of the IEEE*, vol. 67, no. 12, Dec. 1979, pp. 1643–1653.

[30] J. A. Betts and D. R. Ebenezer, "Intermodulation interference in mobile multiple-transmission communication systems operating at high frequencies (3-30) MHz," *Proceedings of the IEE*, vol. 120, no. 11, Nov. 1973, pp. 1337–1343.

[31] W. M. Chase, J. W. Rockway, and G. C. Salisbury, "A method of detecting significant sources of intermodulation interference," *IEEE Transactions on Electromagnetic Compatibility*, vol. 17, no. 2, May 1975, pp. 47–50.

[32] P. Ho, W. S. Wilkinson, and A. C. Tseung, "The suppression of intermodulation product generation in materials and structures used in radio communications," in *IEE Colloquium on Passive Intermodulation Products in Antennas and Related Structures (Digest No. 94)*, London, June 7th, 1989, pp. 5/1–5/5.

[33] P. L. Lui and A. D. Rawlins, "Measurement of intermodulation products generated by structural components," *Electronics Letters*, vol. 24, no. 16, Aug. 1988, pp. 1005–1007.

[34] C. Poulain, L. Boyer, P. Sainsot, M. H. Maitournam, F. Houzé, M. Leclercq, J. P. Guéry, and J. P. Charpentier, "Experimental and theoretical study of creep effects in electrical contacts," in *Proceedings of the 41st Holm Conference on Electrical Contacts 1995*, Montreal, Canada, Oct. 2–4, 1995, pp. 147–153.

[35] K. Kataoka, T. Itoh, and T. Suga, "Characterization of fritting phenomena on Al electrode for low contact force probe card," *IEEE Transactions on Components and Packaging Technologies*, vol. 26, no. 2, June 2003, pp. 382–387.

[36] C. Kittel, *Introduction to Solid State Physics*, 7th ed. New York: John Wiley & Sons, Inc., 1996, 673 p.

[37] R. M. Bozorth, *Ferromagnetism*, 2nd ed. New York: IEEE Press, 1993, 968 p.

[38] P. Robert, *Electrical and Magnetic Properties of Materials*. Norwood, MA: Artech House, Inc., 1988, 458 p.

[39] B. Rosenberger, "Intermodulation testset and high-power measurements," in *IEE Colloquium on Screening Effectiveness Measurements (Ref. No. 1998/452)*, London, May 6, 1998, pp. 3/1–3/34.

[40] G. P. Rodrigue, "A generation of microwave ferrite devices," *Proceedings of the IEEE*, vol. 76, no. 2, Feb. 1988, pp. 121–137.

[41] H. How, C. Vittoria, and R. Schmidt, "Nonlinear intermodulation coupling in ferrite circulator junctions," *IEEE Transactions on Microwave Theory and Techniques*, vol. 45, no. 2, Feb. 1997, pp. 245–252.

[42] D. J. Lynch and B. Pierce, "Third order intermodulation performance of above resonance circulators," in *IEE Colloquium on Advances in Passive Microwave Components (Ref. Number 1997/154)*, London, May 22, 1997, pp. 4/1–4/6.

[43] P. Smith, G. Dolman, T. W. Button, and M. Holker, "Investigations of alternative processing methods in microwave ferrites," in *Proceedings of the 4th International Workshop on Multipactor, Corona and Passive Intermodulation in Space RF Hardware (MULCOPIM2003)*, ESTEC, Noordwijk, Netherlands, Sept. 8–11, 2003, CD-ROM.

[44] H. Tamura, J. Hattori, T. Nishikawa, and K. Wakino, "Third harmonic distortion of dielectric resonator materials," *Japanese Journal of Applied Physics, Part 1*, vol. 28, no. 12, Dec. 1989, pp. 2528–2531.

[45] J. Z. Wilcox and P. Molmud, "Thermal heating contribution to intermodulation fields in coaxial waveguides," *IEEE Transactions on Communications*, vol. 24, no. 2, Feb. 1976, pp. 238–243.

[46] A. von Hippel, *Dielectrics and Waves*, 2nd ed. Boston: Artech House, Inc., 1995, 284 p.

[47] A. Kumar, "Passive IM products threaten high-power satcom systems," *Microwaves&RF*, vol. 26, no. 13, Dec. 1987, pp. 98–103.

[48] G. Ghione and M. Orefice, "Inter-modulation products generation from carbon fibre reflector antennas," in *Proceedings of the IEEE Antennas and Propagation Society International Symposium 1985*, vol. 1, Vancouver, Canada, June 17–21, 1985, pp. 153–156.

[49] S. J. Fiedziuszko, I. C. Hunter, T. Itoh, Y. Kobayashi, T. Nishikawa, S. N. Stitzer, and K. Wakino, "Dielectric materials, devices, and circuits," *IEEE Transactions on Microwave Theory and Techniques*, vol. 50, no. 3, Mar. 2002, pp. 706–720.

[50] Y.-K. Yoon, D. Kim, M. G. Allen, J. S. Kenney, and A. T. Hunt, "A reduced intermodulation distortion tunable ferroelectric capacitor – architecture and demonstration," *IEEE Transactions on Microwave Theory and Techniques*, vol. 51, no. 12, Dec. 2003, pp. 2568–2576.

[51] O. Givati, "Overcoming the passive intermodulation challenge in antenna design," *Antenna Systems & Technology*, no. 2, Mar. 2004, pp. 16–17.

[52] Y. Patenaude, J. Dallaire, F. Ménard, and S. Richard, "Antenna PIM measurements and associated test facilities," in *Proceedings of the IEEE Antennas and Propagation Society International Symposium 2001*, vol. 4, Boston, July 8–13, 2001, pp. 620–623.

[53] P. L. Lui and A. D. Rawlins, "The field measurement of passive intermodulation products," in *5th International Conference on Mobile Radio and Personal Communications, IEE Conference Publication No. 315*, Coventry, UK, Dec. 11–14, 1989, pp. 199–203.

[54] F. S. Sandroff and W. H. Burnett, "Reliability qualification test for circuit boards exposed to airborne hygroscopic dust," in *Proceedings of the 42nd Electronic Components and Technology Conference 1992*, San Diego, USA, May 18–20, 1992, pp. 384–389.

[55] M. Antler, "Survey of contact fretting in electrical connectors," *IEEE Transactions on Components, Hybrids and Manufacturing Technology*, vol. 8, no. 1, Mar. 1985, pp. 87–104.

[56] M. B. Amin and F. A. Benson, "Coaxial cables as sources of intermodulation interference at microwave frequencies," *IEEE Transactions on Electromagnetic Compatibility*, vol. 20, no. 3, Aug. 1978, pp. 376–384.

[57] F. Arazm and F. A. Benson, "Nonlinearities in metal contacts at microwave frequencies," *IEEE Transactions on Electromagnetic Compatibility*, vol. 22, no. 3, Aug. 1980, pp. 142–149.

[58] E. Weibel and U. Hagel, "Tests evaluate the influence of junctions on PIM," *Microwaves & RF*, vol. 37, no. 8, Aug. 1998, pp. 70–80.

[59] F. Suárez, C. Palacios, C. Montesano, and F. Rueda, "A titanium nitride coating tested in passive intermodulation," in *Proceedings of the 4th International Workshop on Multipactor, Corona and Passive Intermodulation in Space RF Hardware (MULCOPIM2003)*, ESTEC, Noordwijk, Netherlands, Sept. 8–11, 2003, CD-ROM.

[60] B. G. M. Helme, "Interference in telecomm systems, from passive intermodulation product generation: an overview," in *Proceedings of the 22nd Antenna Measurement Techniques Association Annual Symposium (AMTA 2000)*, Philadelphia, Oct. 16–20, 2000, pp. 143–149.

[61] P. L. Lui and A. D. Rawlins, "Passive non-linearities in antenna systems," in *IEE Colloquium on Passive Intermodulation Products in Antennas and Related Structures (Digest No. 94)*, London, June 7th, 1989, pp. 6/1–6/7.

[62] J. Sanford, "Passive intermodulation considerations in antenna design," in *Proceedings of the IEEE Antennas and Propagation Society International Symposium 1993*, vol. 3, Ann Arbor, MI, June 28–July 2 1993, pp. 1651–1654.

[63] T. Khattab and A. D. Rawlins, "Principles of low PIM hardware design," in *Proceedings of the Thirteenth National Radio Science Conference*, Cairo, Egypt, Mar.19–21, 1996, pp. 355–362.

[64] C. V. Quiles, B. Mottet, and H. L. Hartnagel, "PIM analysis at waveguide flanges: A theoretical approach," in *Proceedings of the 4th International Workshop on Multipactor, Corona and Passive Intermodulation in Space RF Hardware (MULCOPIM2003)*, ESTEC, Noordwijk, Netherlands, Sept. 8–11, 2003, CD-ROM.

[65] R. Kwiatkowski and M. Vladimirescu, "Modeling microwave contact discontinuities," in *Proceedings of the 34th European Microwave Conference (EuMC 2004)*, Amsterdam, Oct. 12–14, 2004, pp. 289–292.

[66] G. Macchiarella, G. B. Stracca, and L. Miglioli, "Experimental study of passive intermodulation in coaxial cavities for cellular base stations duplexers," in *Proceedings of the 34th European Microwave Conference (EuMC 2004)*, Amsterdam, Oct. 12–14, 2004, pp. 981–984.

[67] M. T. Abuelma'atti, "Prediction of passive intermodulation arising from corrosion," *IEE Proceedings: Science, Measurement and Technology*, vol. 150, Jan. 2003, pp. 30–34.

[68] P. L. Lui, "A study of intermodulation interference due to non-linearities in metallic structures," Ph.D. dissertation, Univ. of Kent, Canterbury, UK, 1990.

[69] N. B. de Carvalho and J. C. Pedro, "A comprehensive explanation of distortion sideband asymmetries," *IEEE Transactions on Microwave Theory and Techniques*, vol. 50, no. 9, Sept. 2002, pp. 2090–2101.

[70] J. Brinkhoff and A. E. Parker, "Effect of baseband impedance on FET intermodulation," *IEEE Transactions on Microwave Theory and Techniques*, vol. 51, no. 3, Mar. 2003, pp. 1045–1051.

[71] V. Golikov, S. Hienonen, and P. Vainikainen, "Effect of impedance loading at higher harmonics on passive intermodulation in antennas," in *Proceedings of the IEEE Antennas and Propagation Society International Symposium 2003*, Columbus, June 22–27, 2003, CD-ROM.

[72] G. L. Heiter, "Characterization of nonlinearities in microwave devices and systems," *IEEE Transactions on Microwave Theory and Techniques*, vol. 21, no. 12, Dec. 1973, pp. 797–805.

[73] M. B. Steer and P. J. Khan, "An algebraic formula for the complex output of a system with multi-frequency excitation," *Proceedings of the IEEE*, vol. 71, no. 1, Jan. 1983, pp. 177–179.

[74] M. B. Steer, P. J. Khan, and R. S. Tucker, "Relationship between Volterra series and generalized power series," *Proceedings of the IEEE*, vol. 71, no. 12, Dec. 1983, pp. 1453–1454.

[75] A. D. Rawlins, J. S. Petit, and S. D. Mitchell, "PIM characterisation of the ESTEC compact test range," in *Proceedings of the 28th European Microwave Conference (EuMC98)*, Amsterdam, Oct. 6–8, 1998, pp. 544–548.

[76] P. L. Aspden, A. P. Anderson, and J. C. Bennett, "Microwave holographic imaging of intermodulation product sources applied to reflector antennas," in *6th International Conference on Antennas and Propagation (ICAP 89), IEE Conference Publication No. 301, Part 1*, Coventry, UK, Apr. 4–7, 1989, pp. 463–467.

[77] J. C. Bennett, A. P. Anderson, P. A. McInnes, and A. J. T. Whitaker, "Microwave holographic metrology of large reflector antennas," *IEEE Transactions on Antennas and Propagation*, vol. 24, no. 3, May 1976, pp. 295–303.

[78] J. Siegenthaler and C. Stäger, "The measurement of microwave intermodulation effects on passive components and system parts," in *Proceedings of the Microwaves and Optoelectronics Conference (MIOP-88)*, Wiesbaden, Germany, Mar. 2–4, 1988.

[79] S. Hienonen, V. Golikov, V. S. Möttönen, P. Vainikainen, and A. V. Räisänen, "Near-field amplitude measurement of passive intermodulation in antennas," in *Proceedings of the 31st European Microwave Conference (EuMC 2001)*, vol. 2, London, Sept. 25–27, 2001, pp. 277–280.

[80] S. Hienonen, P. Vainikainen, and A. V. Räisänen, "Sensitivity measurements of a passive intermodulation near-field scanner," in *Proceedings of the 24th Annual Meeting and Symposium of the Antenna Measurement Techniques Association (AMTA02)*, Cleveland, Ohio, Nov. 3–8, 2002, pp. 294–298.

[81] V. Golikov, S. Hienonen, and P. Vainikainen, "Near-field measurements of passive intermodulation sources in antenna feeding network," in *Proceedings of the 11th Microcoll Conference*, Budapest, Sept. 10–11, 2003, pp. 294–298.

[82] R. J. Mailloux, *Phased array antenna handbook*. Norwood, MA: Artech House, Inc., 1994, 534 p.

[83] N. Fourikis, *Phased array-based systems and applications*. New York: John Wiley & Sons, Inc., 1997, 426 p.

[84] K.-L. Wong, *Compact and broadband microstrip antennas*. New York: John Wiley & Sons, Inc., 2002, 327 p.

[85] C. H. Tsao, Y. M. Hwang, F. Kilburg, and F. Dietrich, "Aperture-coupled patch antennas with wide-bandwidth and dual-polarization capabilities," in *Proceedings of the IEEE Antennas and Propagation Society International Symposium 1988*, vol. 3, Syracuse, NY, June 6–10, 1988, pp. 936–939.

[86] B. Lindmark, S. Lundgren, and C. Beckman, "Dual polarized aperture coupled patch multibeam antenna," in *Proceedings of the IEEE Antennas and Propagation Society International Symposium 1998*, vol. 1, Atlanta, June 21–26, 1998, pp. 328–331.

[87] S.-C. Gao, L.-W. Li, M.-S. Leong, and T.-S. Yeo, "Dual-polarized slot-coupled planar antenna with wide bandwidth," *IEEE Transactions on Antennas and Propagation*, vol. 51, Mar. 2003, pp. 441–448.

[88] G. Dubost, R. Frin, and Y. Bao, "Dual polarized flat array with high isolation for DBS," in *Proceedings of the 1992 International Symposium on Antennas and Propagation*, vol. 1, Sapporo, Japan, Sept. 22–25, 1992, pp. 37–40.

[89] F. Rostan and W. Wiesbeck, "Aperture-coupled microstrip patch phased arrays in C- and X-band – a contribution to future multi-polarization multi-frequency SAR systems," in *Proceedings of the IEEE International Symposium on Phased Array Systems and Technology 1996*, Boston, Oct. 15–18, 1996, pp. 141–146.

[90] H. Valmu, "L-band dual-polarized microstrip patch antennas for an airborne aperture synthesis radiometer," in *Digest of the URSI/IEEE XXII National Convention on Radio Science*, Oulu, Finland, Nov. 20–21, 1997, pp. 33–34.

[91] H. F. Pues and A. R. V. de Capelle, "An impedance-matching technique for increasing the bandwidth of microstrip antennas," *IEEE Transactions on Antennas and Propagation*, vol. 37, no. 11, Nov. 1989, pp. 167–175.

[92] D. M. Pozar, "Finite phased arrays of rectangular microstrip patches," *IEEE Transactions on Antennas and Propagation*, vol. 34, no. 5, May 1986, pp. 658–665.

[93] J.-F. Zürcher, "The SSFIP: A global concept for high-performance broadband planar antennas," *Electronics Letters*, vol. 24, no. 23, Nov. 1988, pp. 1433–1435.

[94] G. A. E. Vandenbosch and A. R. V. de Capelle, “Study of the capacitively fed microstrip antenna element,” *IEEE Transactions on Antennas and Propagation*, vol. 42, no. 12, Dec. 1994, pp. 1648–1652.

[95] D. M. Pozar, “Microstrip antenna aperture-coupled to a microstrip line,” *Electronics Letters*, vol. 21, no. 2, Jan. 1985, pp. 49–50.

[96] ——, “Design considerations for low sidelobe microstrip arrays,” *IEEE Transactions on Antennas and Propagation*, vol. 38, no. 8, Aug. 1990, pp. 1176–1185.

[97] P. Brachat and J. M. Baracco, “Printed radiating element with two highly decoupled input ports,” *Electronics Letters*, vol. 31, no. 4, Feb. 1995, pp. 245–246.